ISRN LUTFD2/TFME - 17/5036 - SE(1-70)
Department of Mechanical Engineering
Division of Mechanics

Optimization of Front Suspension Uprights on a Three-wheeled Electric Vehicle

Ecoist

Oskar Ellerstrand
Tolga Erbay Kilicasan

June 21, 2017

Supervisors:
Thomas Koch
Sirgomez Engineering AB

Solveig Melin
Lund University

Per Lidström
Lund University

Examinator:
Aylin Ahadi
Lund University

For more information:
Division of Mechanics, Lund University, Box 118,
SE-211 00 Lund, Sweden
Homepage: http://www.mek.lth.se/

Copyright © 2017 by Oskar Ellerstrand & Tolga Erbay Kilicasan

Printed by Media-Tryck, Lund, Sweden

Preface

This master thesis was carried out in order to fulfill the final step of the Master degree in Mechanical Engineering. It was performed at the Division of Mechanics at Lund University, Sweden, for Sirgomez Engineering AB, to whom we are very grateful for this opportunity to gain in-depth knowledge about practical usage of the relevant subjects such as vehicle dynamics, multibody dynamics, the finite element method and topology optimization. We would like to express our gratitudes to our supervisors, Thomas Koch at Sirgomez Engineering, as well as Professor Solveig Melin and Professor Per Lidström, our supervisors at Lund University. We would also like to thank our examinator, Profesor Aylin Ahadi. Their support and guidance have been extremely helpful during this period and their technical advices and experiences have helped us to deal with obstacles throughout this master thesis.

A special mention goes to Miljöbron and Malin Planander for distributing the thesis and giving us this opportunity to get familiar with the industry.

We would also like to take the opportunity to thank MSC Software Sweden AB for their online support. Our visit to their office in Gothenburg was very interesting and rewarding, and helped us greatly to make progress with our thesis.

A very big thank you also goes to ANSYS Sweden for their great help and support online during difficult moments.

Last but not least the biggest thanks goes to our families. Their love and support have been the greatest motivation for us to pass the tough challenges encountered during these 5 months.

Abstract

The master thesis was carried out as a part of the project Ecoist at Sirgomez Engineering AB, with the goal of reducing the complexity and mass of the current front suspension upright by designing a new upright from one piece, whilst also considering other aspects such as reliability and manufacturability. In order to achieve this, topology optimization was used. The inputs for the optimization needed from external programs were mainly two things; the loads acting on the upright and a generalized geometry allowing material to be removed.

In order to generate the loads acting on the upright, a multibody model of the Ecoist vehicle was built in Adams/Car, consisting of several different subsystems. The full vehicle assembly was then used for a number of different dynamic drive cases, from which the reaction forces and moments acting on the upright were exported. From all those different load steps, one was chosen as representative for the worst case, which was then used in the optimization.

The generalized geometry was created in Solidworks, using the old upright assembly as reference. The idea was to make it take up as much space as possible without interfering with the surrounding components. The important parts of the geometry, such as the contact surfaces and holes were kept the same, in order to be able to connect the adjacent parts without changing them.

The topology optimization was then performed in Ansys Mechanical with key areas, such as the contact surfaces and holes, excluded from the optimization since they need to retain the same size and shape. The objective function was to minimize the mass whilst the only constraint was a predefined stress limit not to be exceeded of 125 MPa, half of the yield stress for an arbitrary linear elastic material (steel in this case). Afterwards, the optimized geometry had to be smoothed in SpaceClaim in order to obtain a useful geometry, since the optimization output featured undesirably rough surfaces and sharp edges.

The final result is an upright geometry consisting of one piece rather than four pieces assembled by a number of screws. The new upright, proposedly made from aluminum alloy AlSi10Mg, has a mass of 0.9345 kg compared to the original upright assembly, which had a mass of 1.478 kg. This represents a decrease of mass with 36.8%.

Nomenclature

δ_{ij}	The Kronecker delta function
ϵ_{ij}	The strain tensor
$\boldsymbol{\alpha}$	The angular acceleration of a body
$\boldsymbol{\omega}$	The angular velocity of a body
$\boldsymbol{a_{cm}}$	The acceleration of the center of mass of a body
$\boldsymbol{a}$	The displacement colon matrix
$\boldsymbol{F}$	The force sum acting on a body
$\boldsymbol{f}$	The force colon matrix
$\boldsymbol{I_{cm}}$	The moment of inertia tensor of a body
$\boldsymbol{K}$	The stiffness matrix
$\boldsymbol{M_{cm}}$	The moment sum acting around the center of mass of a body
μ	The friction coefficient between brake disc and piston
ν	Poisson's ratio
ω_c	The angular velocity of a brake caliper around the axis of its wheel
ω_w	The angular velocity of a wheel around its axis
ρ	Density
σ_{ij}	The Cauchy stress tensor
σ_{max}	The maximum stress encountered
σ_u	The ultimate stress

σ_y	The yields stress
A_p	The brake piston area
b	The fraction of the total brake pressure applied at the actual brake disc
b_i	The body force vector
c_c	The damper constant for a linear damper for compression
c_e	The damper constant for a linear damper for expansion
D_{ijkl}	The elastic stiffness tensor
E	Young's modulus
F	The resulting force from a spring/damper assembly, defined positive in the compressive direction
f_i	The number of degrees of freedom allowed by joint number i
G	The shear modulus
j	The number of joints in a kinematic chain
k	The spring constant for a linear spring
M	The number of degrees of freedom of a kinematic chain
m	The mass of a body
N	The number of rigid bodies in a kinematic chain, including ground
n_{max}	The maximum powertrain output speed
p	The brake pressure at the actual brake piston
P_{max}	The maximum available drive power
p_{max}	The maximum available brake pressure
r	The effective radius for the brake piston
T_{brake}	The brake torque applied on a wheel
T_{drive}	The drive torque applied on the rear wheel
T_{max}	The maximum available drive torque on the wheel
u_i	The displacement vector

V	Volume
x	The displacement for a spring/damper assembly relative its equilibrium, defined positive in the compressive direction
x_i	The position vector
z_b	The brake input ranging from 0 to 1
z_t	The throttle input ranging from 0 to 1

Contents

1 Introduction **1**
1.1 Background . . . 1
1.2 Objectives . . . 2
1.3 Limitations . . . 2
1.4 Sirgomez Engineering AB . . . 3

2 Statement of the problem **4**

3 Theory **6**
3.1 Adams/Car model . . . 6
3.1.1 Multibody dynamics . . . 6
3.1.2 Input torques . . . 7
3.1.3 Springs, dampers and tyres . . . 8
3.2 ANSYS model . . . 8
3.2.1 Finite element method . . . 8
3.2.2 Topology optimization . . . 9

4 Procedure **10**
4.1 Adams/Car subsystem . . . 11
4.1.1 Wheels . . . 12
4.1.2 Rear suspension . . . 13
4.1.3 Front suspension . . . 15
4.1.4 Steering . . . 17
4.1.5 Body . . . 18
4.1.6 Powertrain . . . 19
4.1.7 Brakes . . . 20
4.2 Adams/Car drive cases . . . 21
4.2.1 Acceleration . . . 21
4.2.2 Braking . . . 21
4.2.3 Constant radius cornering . . . 22
4.2.4 ISO double lane change . . . 22
4.2.5 Acceleration during cornering . . . 22
4.2.6 Braking during cornering . . . 22
4.3 Choosing a representative worst load case . . . 22

4.4 Generalized CAD-geometry 23
4.5 FEM setup 25
4.6 Topology optimization 28
4.7 Reverse engineering 29
4.8 Validation 30

5 Results and discussion **32**
5.1 Adams/Car 32
5.2 Ansys 35

6 Summary of the results **43**

7 Future work **45**

APPENDICES **48**

A Lists of joints **49**

B Tyre files **51**

C Load curves **56**

D Matlab code - Powertrain **61**

E Matlab code - Worst load case **62**

List of Figures

2.1 The current upright assembly. 4
2.2 The current upright assembly, seen from behind. 5

4.1 The Adams/Car assembly. 12
4.2 The rear wheel template. 13
4.3 The front wheel template. 13
4.4 The rear suspension template. 15
4.5 The front suspension template. 17
4.6 The steering template. 18
4.7 The body template. 19
4.8 The powertrain template. 20
4.9 The brake system template. 21
4.10 The generalized geometry used for the topology optimization. . . 24
4.11 The generalized geometry used for the topology optimization, seen from behind. 24
4.12 The fixed regions are shown in blue, with the surfaces with loads applied are shown as red. 25
4.13 The fixed regions are shown in blue, with the surfaces with loads applied are shown as red, seen from behind. 26
4.14 The meshed basic geometry for the optimization. 27
4.15 The meshed basic geometry for the optimization, seen from behind. 27
4.16 The basic excluded regions in the optimization marked in red. . . 28
4.17 The basic excluded regions in the optimization marked in red, seen from behind. 29
4.18 The mesh of the final geometry used for validation. 30
4.19 The mesh of the final geometry used for validation, seen from behind. 31

5.1 The magnitude of the different forces acting on the upright during different drive cases. Gray lines represent transition to the next drive case, ordered in the same way as presented in table 5.3. . . 34

5.2 The magnitude of the different moments acting on the upright during different drive cases. Gray lines represent transition to the next drive case, ordered in the same way as presented in table 5.3. 34
5.3 The result of the initial finite element analysis of the generalized geometry at the representative worst load step. 36
5.4 The result of the initial finite element analysis of the generalized geometry at the representative worst load step, seen from behind. 36
5.5 The maximum stress in the initial finite element analysis of the generalized geometry, plotted versus load step. 37
5.6 The output from the topology optimization. 37
5.7 The output from the topology optimization, seen from behind. . 38
5.8 The optimized geometry smoothed in SpaceClaim. 39
5.9 The optimized geometry smoothed in SpaceClaim, seen from behind. 40
5.10 The result of the validation with maximum stresses. 41
5.11 The result of the validation with maximum stresses, seen from behind. 41
5.12 The maximum stress in the initial finite element analysis of the optimized geometry, plotted versus load step. 42

C.1 The x, y and z components of the upper link force for each load step. Gray lines represent transition to the next drive case, ordered in the same way as presented in table 5.3. 56
C.2 The x, y and z components of the lower link force for each load step. Gray lines represent transition to the next drive case, ordered in the same way as presented in table 5.3. 57
C.3 The x, y and z components of the tierod force for each load step. Gray lines represent transition to the next drive case, ordered in the same way as presented in table 5.3. 57
C.4 The x, y and z components of the caliper upper force for each load step. Gray lines represent transition to the next drive case, ordered in the same way as presented in table 5.3. 58
C.5 The x, y and z components of the caliper lower force for each load step. Gray lines represent transition to the next drive case, ordered in the same way as presented in table 5.3. 58
C.6 The x, y and z components of the caliper translational force for each load step. Gray lines represent transition to the next drive case, ordered in the same way as presented in table 5.3. 59
C.7 The x, y and z components of the upper link torque for each load step. Gray lines represent transition to the next drive case, ordered in the same way as presented in table 5.3. 59
C.8 The x, y and z components of the lower link torque for each load step. Gray lines represent transition to the next drive case, ordered in the same way as presented in table 5.3. 60

C.9 The x, y and z components of the caliper rotational torque for each load step. Gray lines represent transition to the next drive case, ordered in the same way as presented in table 5.3. 60

List of Tables

4.1 The parameters used for calculating the forces from the rear spring/damper assembly. 14
4.2 The parameters used for calculating the forces from the front spring/damper assemblies. 16
4.3 The parameters used for calculating the drive torque. 19
4.4 The parameters used for calculating the brake torques. 20
4.5 Material data for structural steel 28
4.6 Material data for AlSi10Mg 31

5.1 Calculation of number of bodies 32
5.2 Calculation of degrees of freedom 32
5.3 The way that the drive cases are ordered in the load diagrams. . 33
5.4 The forces acting on the upright in the chosen "worst load case" that is used as input for the topology optimization 35
5.5 The moments acting on the upright in the chosen "worst load case" that is used as input for the topology optimization 35

6.1 Comparison of the volumes and masses of the different versions of the upright. 43

A.1 List of joints in the rear suspension subsystem 49
A.2 List of joints in the rear wheel subsystem 49
A.3 List of joints in the steering subsystem 49
A.4 List of joints in the front suspension subsystem 50
A.5 List of joints in the front wheels subsystem 50

Abbreviations

General

CAD: Computer aided design

DOF: Degree(s) of freedom

FEM: Finite element method

Tables

B: Body

RS: Rear suspension

RW: Rear wheel

S: Steering

FS: Front suspension

FW: Front wheels

SF: Safety factor

Chapter 1

Introduction

1.1 Background

The first electric vehicle was built by the British electrical engineer Thomas Parker in London in 1884 and was powered by his own-designed high-capacity rechargeable batteries. The term "electric vehicle" refers to any vehicle that uses electric motors for propulsion[1]. Electric vehicles compose today a small part of all vehicles on traffic in the world but more effort is devoted to development and progress is made upon this.

As previously mentioned there is a variety of electrical vehicles on the market today and depending on the customer's need you can either choose an electric bike and motorcycle or a hybrid car driven by both electricity and another propellant (commonly a combustion engine). The latest offer today is to choose a car driven by only electricity, such as Tesla. "Tesla was founded in 2003 by a group of engineers in Silicon Valley who wanted to prove that electric cars could be better than gasoline-powered cars."[2] One of the biggest advantages is the fact that electric-power has zero direct emission of harmful particles. Since our world faces severe damages from the pollution from vehicles driven by fossil fuels such as gasoline and diesel, it is of vital interest to make a change in order to protect our planet.

The idea behind the project is based on how human beings transport themselves to pursue their daily routines. Car, bus and train are the three most common transportation forms of modern society. Most of the transportations are done alone or at a short range, especially when people are going to work by cars. The fact that transportation is done alone is a major problem and the consequences are even worse. Instead of driving a car to work lonely it is more advantageous to choose carpooling and thus reduce further pollution to the planet. However, carpooling could be difficult to manage and a more effective way could instead

be a single-passenger vehicle driven by pure electricity. This will surely decrease the needed space and mass for a vehicle and should cause less destruction to the earth.

This master thesis concerns the vehicle Ecoist, presently under development at Sirgomez Engineering AB. Ecoist is a motorcycle registered three-wheeled vehicle with so called tadpole configuration, i.e. 2 wheels at the front and one single wheel at the rear[3]. The goal is to carry one single passenger and a bag of about 20 kg. In comparison to other established three-wheelers Ecoist uses electric-powertrain and its wheel configuration has better driving dynamics than more common delta configuration of one single wheel at the front and 2 wheels at the rear. The tadpole configuration has several advantages such as potentially improved aerodynamics and better stability, since the maximum tyre friction is normally extracted during braking and cornering, but not during acceleration. Every battery charge will last an approximate range of about 50-80 km. The top speed is set to 90 km/h and the net weight of Ecoist is desired to be 300 kg, located as such that each wheel carries approximately 100 kg.

1.2 Objectives

The main objective of this master thesis is to propose an improved version of the upright at the front suspension with regards to complexity and mass, whilst also considering aspects such as reliability and manufacturability. The strategy for achieving this objective is to run a topology optimization with mass minimization as the objective, whilst constraining the stresses. Necessary inputs for the topology optimization are the loads acting on the upright, as well as an initial geometry.

The loads acting on the upright have to be calculated from the multibody system from several different relevant drive cases, which also have to be determined. Meanwhile the initial geometry for the optimization has to be based on the current upright with regards to the contact surfaces where the contact forces shall be applied as well as not interfering with other components in the suspension, while limiting the end result as little as possible. The multibody model will be built and analysed in Adams/Car, whilst the CAD-geometry will be created in SolidWorks. The finite element analysis and the topology optimization will then be carried out in Ansys Mechanical.

1.3 Limitations

The model created in Adams/Car composes several subsystems, which in turn also consist of a huge number of smaller parts. These parts are (apart from the tyres, springs and dampers) approximated as rigid bodies in order to simplify

calculations. The existing CAD-model created in Solidworks is far more detailed as it consists of small parts which are bolted together to form close-to-rigid parts. Thus modelling these parts as finite element bodies in Adams/Car would require much more work and would yield potentially much slower calculations, for little benefit. Also, no bushings were used as the stiffness of the real bushings were not known, and it was estimated not to be of great importance.

The brake input acting on each wheel/hub/rim in Adams/Car is only a resultant moment, but in reality a resultant force also appears. The influence from this resultant force is thus ignored.

The power input is acting as a pure torque on the rear wheel axis, but in reality the torque is produced around an axis where the motor is placed, and transferred to the rear wheel axis through a belt, introducing a force at an eccentric position giving cause not only to the moment but also a resultant force. This could have been modeled more detailed, requiring more simulation and setup time, but this resultant force was also assumed negligible.

The current suspension components, especially the hub, limits the initial upright geometry in order to avoid interference.

The finite element simulations feature fixed surfaces in the contact region with the ball bearings, rather than simply the reactions forces and allowing the entire body to accelerate, in order to simplify the simulations. The body forces are also assumed to be negligible in comparison to the contact forces.

1.4 Sirgomez Engineering AB

The consultant company Sirgomez Engineering AB develops and finances selected projects in design-controlled products primarily in vehicles. Meanwhile education is offered to clients in order to earn more knowledge about vehicle dynamics and design. In 1999 the company was established in Germany by Thomas Koch, the current CEO, and in 2002 he moved to Sweden. From that time until now he has been working in many different companies like Volvo Cars/Trucks, Najad Yachts, Highland Motors, Industrilås, Marinediesel, Koenigsegg, Hammerglass and Blackwing. In addition to the mentioned companies above Koch has been involved in several smaller corporations and projects.

Sirgomez Engineering AB possesses all rights of Ecoist and it is the company's first own product entirely financed by themselves. The construction of the vehicle started approximately 2 years ago and they have been successful during these years. Now they need some assistance by master thesis students to further analyze some parts of the vehicle.

Chapter 2

Statement of the problem

The major task of this master thesis is to optimize the geometry of the suspension upright with respect to complexity and mass, without compromising reliability and manufacturability. The main focus will lie on minimizing the mass through minimizing the volume, with the choice of material coming in second hand. This will be achieved by simulations in Adams/Car for obtaining the loads acting on the upright and topology optimization in Ansys Mechanical in order to get the final geometry. The current upright has the following geometry:

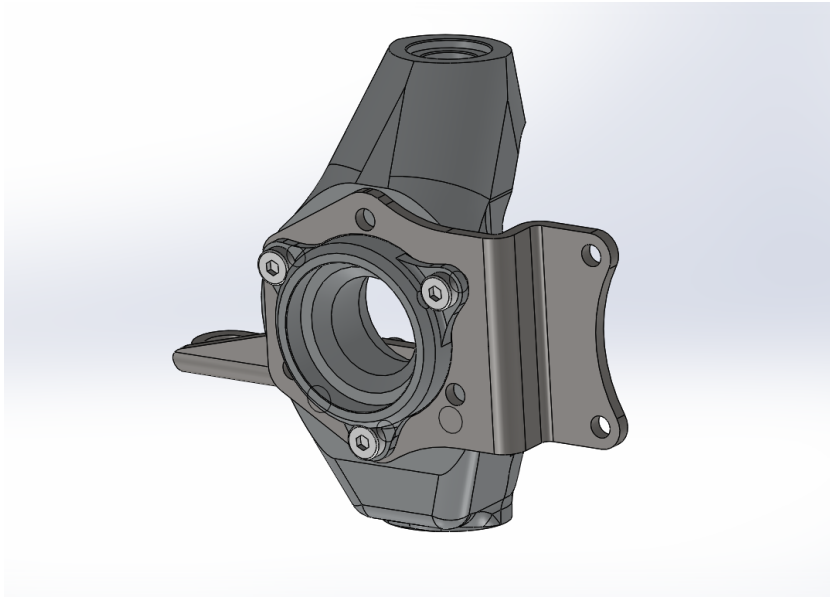

Figure 2.1: The current upright assembly.

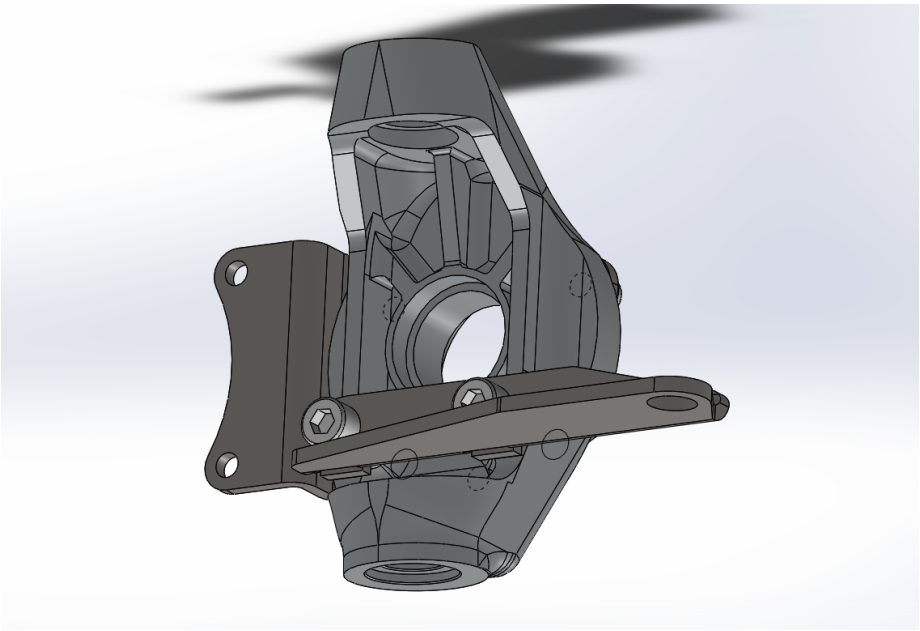

Figure 2.2: The current upright assembly, seen from behind.

Chapter 3

Theory

3.1 Adams/Car model

Adams/Car needs to be used in order to obtain the loads acting on the suspension upright for a number of different drive cases. The program uses multibody dynamics, and closes the equations through the contacts with the ground with a tyre model. Brake input and throttle input respectively are converted into brake torques and driving torques, which need to be modeled.

3.1.1 Multibody dynamics

As previously mentioned, only rigid bodies will be used in the simulations carried out in Adams/Car. The multibody system consists of a number of rigid bodies which, had they been unaffected by constraints, each would have had six degrees of freedom for general spatial motion in the 3D space (3 translational and 3 rotational). For each rigid body, six equations of motion can be set up either through the Newton-Euler equations or Lagrange's equations. The Newton-Euler equations for one rigid body can be expressed in vector form as follows (with the moment equation taken around the center of gravity for the body)[4]:

$$\boldsymbol{F} = m\boldsymbol{a}_{cm} \tag{3.1}$$

$$\boldsymbol{M}_{cm} = \boldsymbol{I}_{cm}\boldsymbol{\alpha} + \boldsymbol{\omega} \times \boldsymbol{I}_{cm}\boldsymbol{\omega} \tag{3.2}$$

The degrees of freedom are constrained by connections between the bodies through joints, which reduces the number of degrees of freedom. The Chebychev-Gruebler-Kutzbach criteria (also known as the mobility formula or simply

Greubler's equation) states that the total number of degrees of freedom for a three-dimensional kinematic chain is[5]:

$$M = 6(N-1) - \sum_{i=1}^{j} 6 - f_i = 6(N-1-j) + \sum_{i=1}^{j} f_i \tag{3.3}$$

It shall be noted that the Chebychev-Gruebler-Kutzbach criteria cannot be used without care. For example, for an overconstrained mechanism the actual number of degrees of freedom will be more than that predicted by the mobility formula, as the reaction loads become statically indeterminate.

The multibody system regarding a three wheeled vehicle with steering (without interlinked suspension systems such as anti roll bars) should have 7 degrees of freedom relative the body of the car; one rotational for each wheel, one for suspension travel for each wheel, and finally one for the steering.

3.1.2 Input torques

In Adams/Car, the standard brake system is using a simplified mathematical model which does not take into account for the complicated interactions between the disc and the caliper. It instead works by only applying a resultant brake torque (and no resultant force) for each wheel (with a reaction torque acting on the calipers mounted on the uprights) calculated as:

$$T_{brake} = 2A_p p\mu r \, sign(\omega_w - \omega_c) \tag{3.4}$$

Where the brake line pressure is calculated according to:

$$p = z_b b p_{max} \tag{3.5}$$

The powertrain can be modeled in different ways. The most convenient way is to use the simple-mode in the Adams-model which features a simplified powertrain and an idealized cvt transmission which allows the motor to reach its maximum power output for all angular velocities above a certain value, which is limited by the maximum torque output that becomes active for lower angular velocities, in accordance with:

$$T_{drive} = z_t \, min(T_{max}, \frac{P_{max}}{\omega_w}) \tag{3.6}$$

Thus by limiting the maximum angular acceleration and setting the maximum power to more than the maximum torque times the limited angular acceleration, it can be ensured that the set torque limit is always active, leading to a constant maximum output torque.

$$T_{drive} = z_t T_{max} \tag{3.7}$$

Just as for the brake system, a reaction torque is also applied, in this case on the rigid chassis. A differential is also included in the standard powertrain model, however this is not needed for one-wheel-drive. Thus the output driving torque will only be applied to one wheel rather than split through a mathematical differential and applied to two separate wheels[6].

3.1.3 Springs, dampers and tyres

The springs and dampers are the only flexible parts in the Adams/Car model within the chassis. The force from a spring is only displacement dependent while the damper force is only depending on the relative displacement velocity. Their respective dependencies are linear in this case, however the damper behaves differently depending on whether it is compressing or extending, leading to equation 3.8.

$$F = \begin{cases} kx + c_e\dot{x} & if \;\; \dot{x} < 0 \\ kx + c_c\dot{x} & if \;\; \dot{x} > 0 \end{cases} \tag{3.8}$$

Finally, the tyres are arguably the most complex part of the entire Adams/Car simulation. Many different models are available, but one of the most common models is the Pacejka '89 tyre model, based on the Pacejka Magic Formula. The normal tyre force is calculated by assuming deformation behaviour in an identical way as for a linear spring and damper, thus equation 3.8 can be used for that too.

All other contact forces and moments for each tyre are based on the vertical force, as well as slip and slip angles, through the Pacejka Magic Formula. For details regarding these calculations, see the Adams/Tyre manual[7].

3.2 ANSYS model

Ansys Mechanical will be used in order to optimize the upright geometry with finite elements, and later to validate the optimized geometry.

3.2.1 Finite element method

The finite element method is a numerical method for solving the general differential equations present in the mechanical problem, written on Einstein notation (assuming a non-accelerating body)[8]:

$$\begin{cases} \frac{\partial \sigma_{ij}}{\partial x_j} + b_i = 0 \\ \epsilon_{ij} = \frac{1}{2}(\frac{\partial u_i}{\partial x_j} + \frac{\partial u_j}{\partial x_i}) \\ \sigma_{ij} = D_{ijkl}\epsilon_{kl} \end{cases} \tag{3.9}$$

where for linear elastic materials:

$$D_{ijkl} = 2G\left[\frac{1}{2}(\delta_{ik}\delta_{jl} + \delta_{il}\delta_{jk}) + \frac{\nu}{1-2\nu}\delta_{ij}\delta_{kl}\right] \tag{3.10}$$

and where:

$$G = \frac{E}{2(1+\nu)} \tag{3.11}$$

This is done by dividing the geometry into small elements for a finite element analysis. The finite element formulation is obtained through the weak formulation, and eventually lead to a matrix equation on the following form:

$$\boldsymbol{Ka} = \boldsymbol{f} \tag{3.12}$$

where either the displacement of a node, or the force of a node can be calculated, depending on what is known. The only known values are those on the boundaries, from the boundary conditions, where either the displacement or the forces are known. From the equation the displacements become known at all node points, and from that both the strain distribution and perhaps more importantly the stress distribution can be obtained through equation 3.9.

3.2.2 Topology optimization

Topology optimization is a method to mathematically optimize a mechanical structure by allowing material to be reduced from the initial geometry. It is based on the finite element method and requires an objective function as well as constraints. It works by introducing a pseudo-density as the design variable for each element, that represents how much of the material in that element that is being kept. Reducing the pseudo-density in an element thus also reduces the stiffness. The result of a topology optimization is the pseudo-density field, scaling from 0 to 1 and by setting a limit for what material to include, an optimized geometry can be obtained.

Chapter 4

Procedure

As previously mentioned, the task of the thesis is to minimize the mass of the upright. This will be done with topology optimization in Ansys Mechanical. However, a number of things are needed before an optimization can be carried out, as listed below:

- Boundary conditions
- Geometry
- Material
- Objective and constraint(s)
- Mesh

The boundary conditions needed are the reaction forces and moments acting on the upright when driving. These will be extracted from vehicle simulations in Adams/Car, using multibody dynamics for a number of different drive cases. However, only one load step can realistically be used in the optimization, thus a representative worst load case will need to be singled out.

Furthermore, an input geometry for the optimization needs to be created in a CAD-program such as Solidworks, based on the existing geometry but more generalized, allowing material to be removed in the optimization. Additionally a material needs to be chosen for the optimization, as well as objectives and constraints, and a mesh.

Finally after the optimization, the optimized geometry needs to be cleaned and smoothened in order to be useful, whereafter it can be validated.

The procedure can be summed up in the following steps:

- Adams/Car subsystems
- Adams/Car drive cases

- Choosing a representative worst load case
- Generalized CAD-geometry
- FEM setup
- Topology optimization
- Reverse engineering
- Validation

4.1 Adams/Car subsystem

The multibody system is created in Adams/Car through eight different subsystems, as listed below:

- Front wheels
- Rear wheel
- Front suspension
- Rear suspension
- Steering
- Body
- Powertrain
- Brakes

Every part mentioned above consists of joints in order to lock the relative motion between parts where necessary. After assembling the different subsystems together, a number of different full-vehicle analyses are carried out. The entire vehicle assembly can be seen in figure 4.1. For a list of all joints present in the entire vehicle, see appendix A.

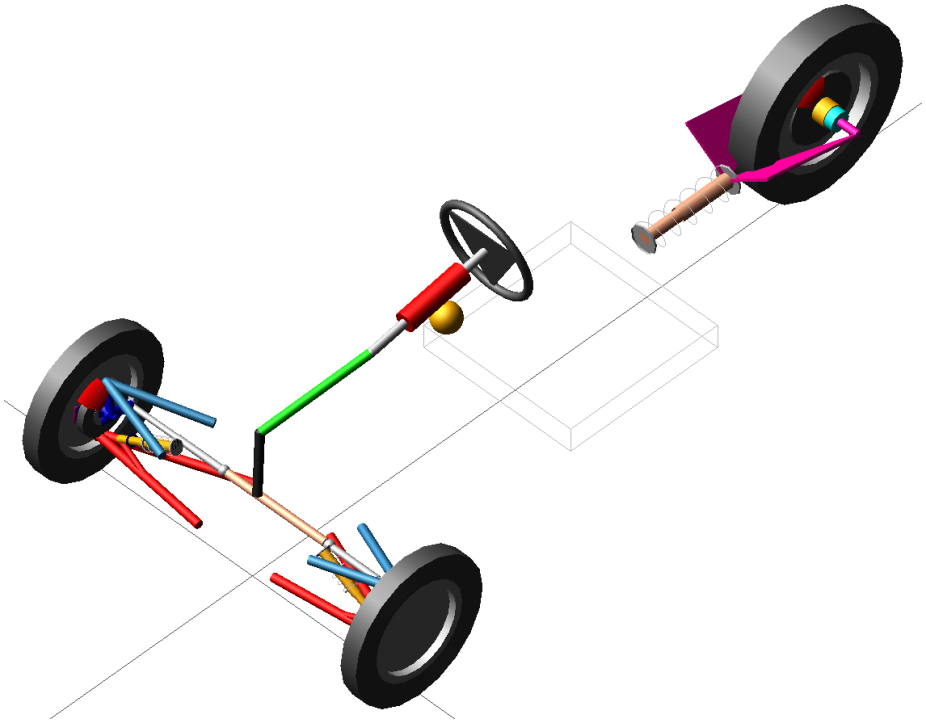

Figure 4.1: The Adams/Car assembly.

4.1.1 Wheels

The front wheels template is based on the standard template 'handling_tires'. Meanwhile the rear tyre template is built from scratch since there is no standard template of one single wheel.

The tyre properties for both templates have to be set to the relevant values for the actual tyres used by Ecoist. Due to a lack of tyre data, the recommended values from [9] are used, with the exception of the friction coefficients, which are set to 0.8. The size and mass properties are based on the CAD-files.

Each wheel has a fixed joint to a mount part in its suspension subsystem, i.e. its hub (front) or rim (rear). The used tyre parameters can be found in the code in appendix B. Figure 4.2 illustrates the rear wheel, while the front wheels template can be seen in figure 4.3.

Figure 4.2: The rear wheel template.

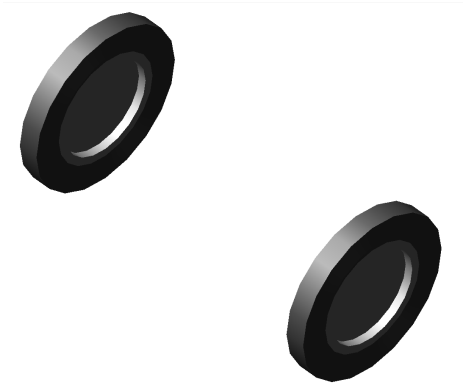

Figure 4.3: The front wheel template.

4.1.2 Rear suspension

The rear suspension has to be created from scratch in Adams/Car Template Builder. It consists of the following parts:

- forward damper half (invisible)
- rearward damper half (invisible)
- swing arm (magenta)
- rim (cyan)

Additionally, the following items are also included:

- damper (peach)
- spring (white)

However these are not real 'parts' in Adams, but only act as forces applied through property files, as a function of displacement or velocity between the two damper halves.

The rim is connected to the swing arm through a revolute joint, allowing the rear wheel to rotate. The swing arm in turn is connected to the body via a revolute joint, as well as to the rearward damper half through a hooke joint. The forward damper half is connected to the body through a hooke joint. The damper halves are connected to each others through a cylindrical joint.

Parameters regarding the subsystem are summarized in table 4.1 Note that the spring constant changes from k_1 to k_2 at x_{1-2}. From figure 4.4 it can be seen what the rear suspension looks like.

Rear suspension parameters		
k_1	225.6	(N/mm)
k_2	294	(N/mm)
x_{1-2}	28.8	(mm)
c_e	11.251	(Ns/mm)
c_c	3.387	(Ns/mm)

Table 4.1: The parameters used for calculating the forces from the rear spring/-damper assembly.

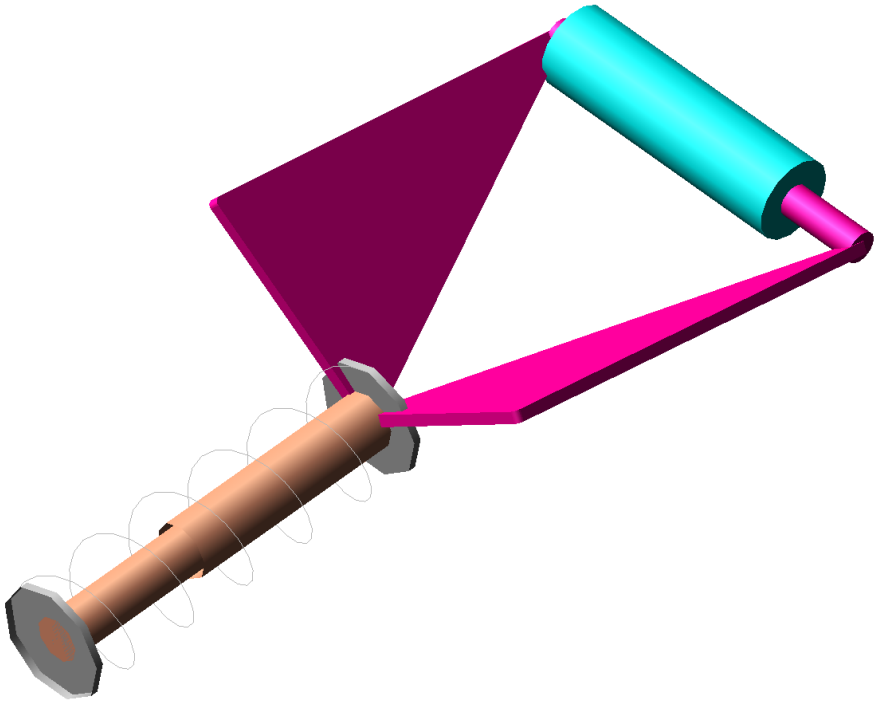

Figure 4.4: The rear suspension template.

4.1.3 Front suspension

The front suspension of Ecoist is a simple 'double_wishbone' which is based on the existing template and it consists of the following parts (two of each due to symmetry):

- lower damper halves (invisible)
- upper damper halves (invisible)
- upper A-arms (light blue)
- lower A-arms (red)
- tie rods (silver)
- hubs (dark grey)
- uprights (dark blue)

In order to calculate the forces acting on the upright at the correct positions, each upright had to be extended by three new rigid bodies, with a fixed joint to the main upright for each new part. The new bodies are:

- upper upright links (peach)
- lower upright links (green)
- brake calipers (magenta)

Additionally the following items (not parts in Adams as was explained previously) are also included in the front suspension:

- dampers (yellow)
- springs (white)

They act as forces applied at the damper halves through property files, as a function of displacement or velocity between the two damper halves.

Each hub is mounted to an upright through a revolute joint, allowing the hub and wheel to rotate. The upright is as previously mentioned extended with fixed joints to three other bodies. The upper link is connected to the upper wishbone whilst the lower link is connected to the lower wishbone, both through spherical joints. Both wishbones are then connected to the body (mount part) through revolute joints. Meanwhile the tie rod is connected to the upright with a spherical joint in one end and the steering rack (mount part) through a convel joint in the other. Finally, the lower damper part is connected to the lower wishbone with a hooke joint, and the upper damper part to the body through a hooke joint as well. The two damper halves can move relative one another through a cylindrical joint.

The parameters regarding the spring/damper assembly can be found in table 4.2. Figure 4.5 illustrates the double wishbone suspension with its components.

Front suspension parameters		
k	105.08	(N/mm)
c_e	11.251	(Ns/mm)
c_c	3.387	(Ns/mm)

Table 4.2: The parameters used for calculating the forces from the front spring/-damper assemblies.

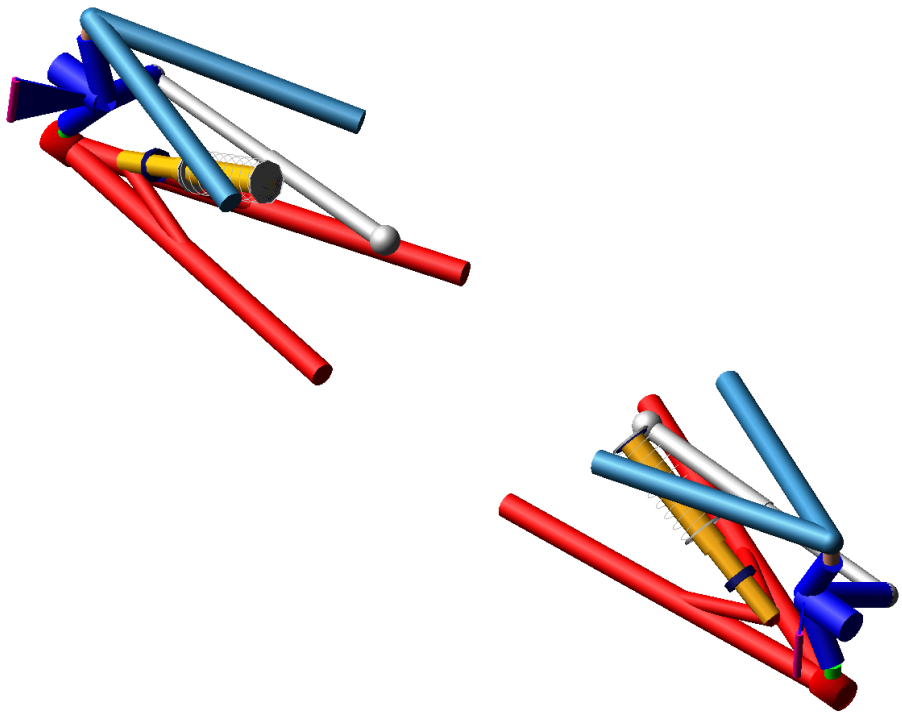

Figure 4.5: The front suspension template.

4.1.4 Steering

The steering system is based on the standard from the template library which is called 'rack_pinion_steering'. It consists of following components:

- steering wheel (dark grey)
- steering column (silver)
- intermediate shaft (green)
- pinion shaft (black)
- rack (blue)

Also visible are two mount parts representing parts of the body:

- column support (red)
- rack housing (peach)

The column support is connected to the steering column via a cylindrical joint. The steering wheel in turn is fixed to the steering column. The intermediate

shaft lies in between the steering column and the pinion shaft, and is connected to both through hooke joints. The rack housing (mount part) supports the rack through a translational joint, as well as the pinion shaft through a revolute joint. Those two joints are connected with a gear, forcing the rotational motion and translational motion to be connected, reducing one degree of freedom. Figure 4.6 illustrates the rack and pinion steering with its components.

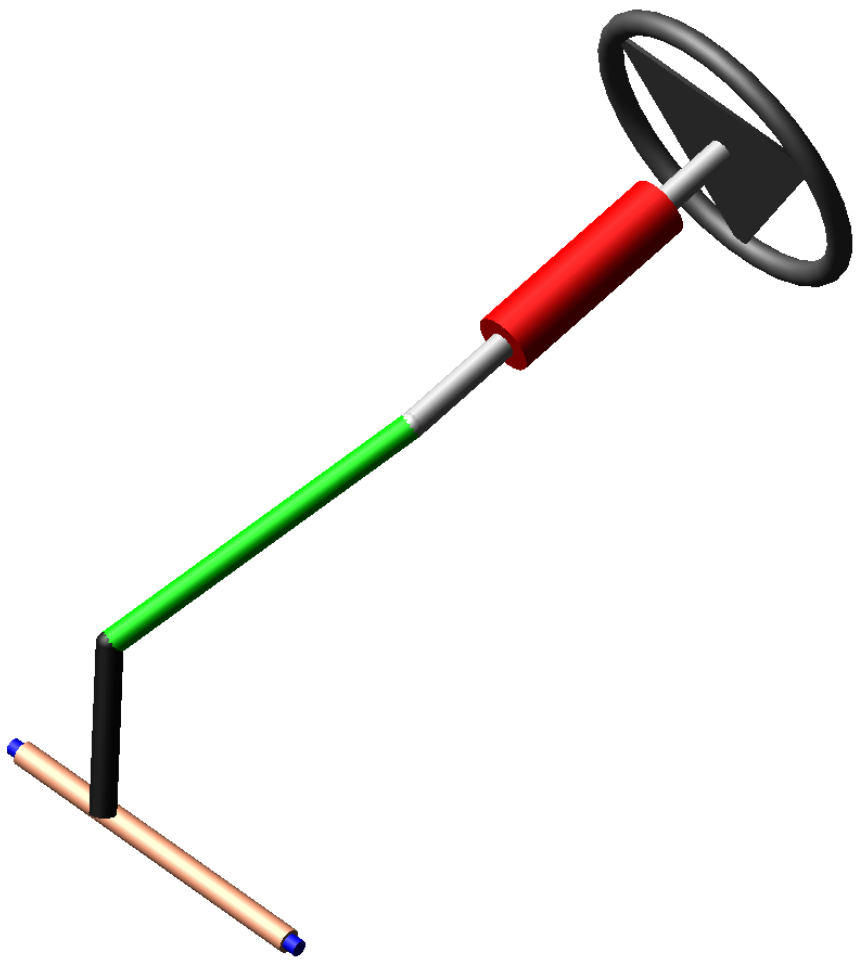

Figure 4.6: The steering template.

4.1.5 Body

The body of Ecoist is selected from the templates as 'rigid_chassis_it' and is a rigid body with no direct visible parts (only the center of mass). The purpose

of the chassis is to connect the other subsystem (front and rear suspension, and steering) through a rigid body, whilst having important mass and inertia properties. The rear suspension is connected to the body through a revolute joint to the swing arm and a hook joint to the damper. The front suspension is connected through two revolute joints for the upper and lower wishbone respectively, and a hooke joint to the damper. The steering system is connected to the rack (translational joint) and the steering column (cylindrical joint). Figure 4.7 illustrates the body of the vehicle.

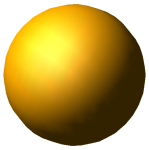

Figure 4.7: The body template.

4.1.6 Powertrain

The powertrain had to be heavily modified from the standard template ('powertrain') in order to be adapted to Ecoist, due to its one wheel drive which reduces the need of a differential. Also the electric motor features different power properties than a combustion engine which is used in the standard template, which thus also needed to be modified. The output torque is applied to the rim in the rear suspension subsystem, with a reaction torque acting on the body. The output torque is calculated with equation 3.7 and uses the parameters from table 4.3. For the calculations of these parameters, see appendix D. The Adams model of the powertrain can be seen in figure 4.8.

Powertrain parameters		
T_{drive}	213380	(Nmm)
n_{max}	881	(RPM)

Table 4.3: The parameters used for calculating the drive torque.

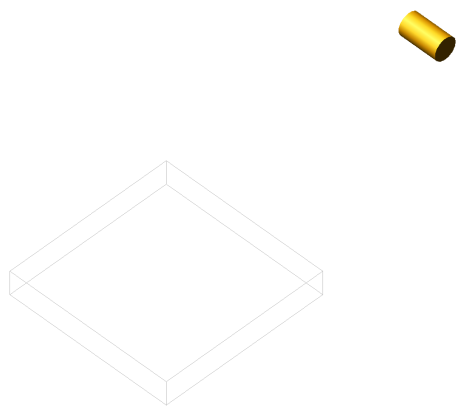

Figure 4.8: The powertrain template.

4.1.7 Brakes

The brake subsystem also had to be modified in order to comply with the three-wheeled Ecoist, by replacing the two symmetry-based brakes with one single. The braking torque is applied to each wheel, with a reaction torque acting on each braking caliper in the front suspension subsystem for the front brakes and on the swing arm in the rear suspension subsystem for the rear brake. The brake torque is calculated in accordance equation 3.4 with data from table 4.4. The brakes model can be seen in figure 4.9.

Brake parameters		
μ	0.4	
$A_{p,f}$	633.15	(mm^2)
$A_{p,r}$	1139.5	(mm^2)
r_f	95	(mm)
r_r	124	(mm)
p_{max}	6.3498	(MPa)
b_f	0.4080675	
b_r	0.183865	

Table 4.4: The parameters used for calculating the brake torques.

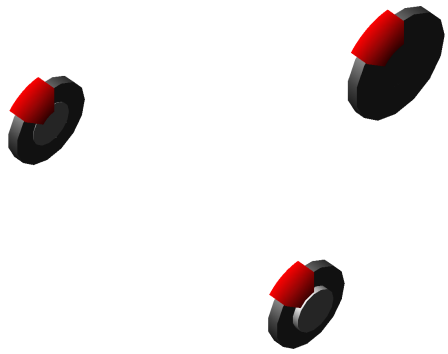

Figure 4.9: The brake system template.

4.2 Adams/Car drive cases

The following drive cases are included in the study:

- Acceleration
- Braking
- Constant radius cornering
- ISO double lane change
- Acceleration during cornering
- Braking during cornering

All drive cases are simulated on an even, plane surface, since no tyre model is currently capable of capturing sudden bumps in a satisfying way.

4.2.1 Acceleration

The acceleration case starts from 5 km/h and steps the throttle input from 0 to 1 during 0.5 seconds. The steering is locked straight and the brakes are not active. The drive case ends when the car reaches its top speed (90 km/h).

4.2.2 Braking

The braking case starts from the top speed of 90 km/h and the braking input steps from 0 to 1 during 0.5 seconds. Just as for the acceleration case, the steering is locked. The throttle input is 0 all way through. The drive case ends when the car slows down to 5 km/h.

4.2.3 Constant radius cornering

The case of constant radius cornering starts with driving forwards before the steering input is stepped from 0 to 30 degrees left on the steering wheel in 0.5 seconds. Both the throttle input and the brake input are zero during the case, with an initial speed of 70 km/h.

4.2.4 ISO double lane change

In the ISO double lane change case, the steering input is following a predetermined curve, consisting of first a lane change from right file to left file, and then after a while changing back to the right file again, simulating an overtaking maneuver. The brake and throttle inputs are used to ensure that the speed is maintained at around 70 km/h.

4.2.5 Acceleration during cornering

The case of acceleration during cornering starts out with the car driving straight in 5 km/h. Then the steering input steps to 30 degrees left on the steering wheel during 0.5 seconds. After a short period of 0.5 seconds to let the shock settle, the throttle input steps from 0 to 1 during 0.5 seconds. The case ends when the car reaches its top speed (90 km/h) or slides to a stop.

4.2.6 Braking during cornering

The case of braking during cornering starts out with the car driving straight in 90 km/h. Then the steering input steps to 30 degrees left on the steering wheel during 0.5 seconds. After a short 0.5 second period to let the shock settle, the brake input steps from 0 to 1 during 0.5 seconds. The case ends when the car slows down to 5 km/h.

4.3 Choosing a representative worst load case

After obtaining the forces and moments acting on the upright as a discrete function of time for each drive case, a representative worst load case needs to be found in order to be used as a reasonable input of contact loads for the optimization. The reason for this is that all load steps cannot be used as input for the optimization, since that would require too much computing effort.

However, before doing that, the reaction force and torque acting on the brake caliper through a fixed joint in Adams/Car need to be recalculated to the two mounting holes for the brake caliper. Ideally, this would turn out to be one force

on each hole. However this is not possible since the moment in the direction between the holes could not possibly be retained. Thus this moment needs to be retained and is distributed equally to both holes. The force in the direction between the holes also has to be distributed equally to both holes, as there is not possible to say how much of it belongs to which hole, as this is a problem of statical indefiniteness.

This is not straightforward since it is not obvious which load case is the worst. One method is to, for each load step, simply add the force magnitudes from all forces, and then single out the largest sum as the worst load step, whilst neglecting the moments. Another way would be to consider the moments by dividing the magnitudes with a characteristic length and then add in the same way as the force magnitudes, however this characteristic length would be rather arbitrary and yet have a big influence on the outcome. The way the reaction force and torque is recalculated can be seen in appendix E.

In the end it is decided that simply adding the force magnitudes will be adequate, and regardless of the input for the topology optimization, validation will show if other load cases will affect the optimized geometry in a worse manner.

4.4 Generalized CAD-geometry

The next step is to create a new CAD-model of the upright in Solidworks, consisting of only one single part instead of an assembly of several parts. This is done by basing the new model on the current one, that consists of several parts, by measurements and deciding what key parts of the geometry that need to be kept. The new generalized geometry can be seen in figures 4.10 and 4.11.

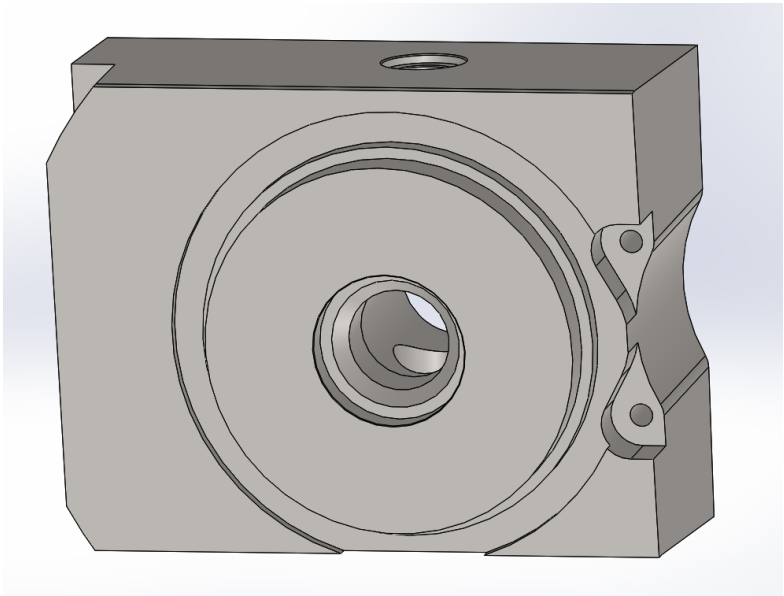

Figure 4.10: The generalized geometry used for the topology optimization.

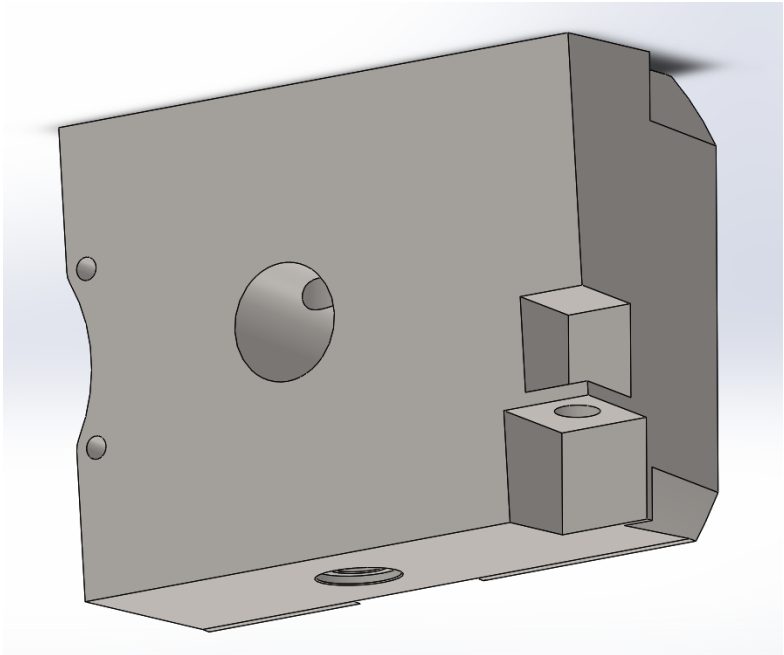

Figure 4.11: The generalized geometry used for the topology optimization, seen from behind.

This model is then imported to Ansys Mechanical. Thus no contact conditions within the upright have to be set and the upright structure gets a more general geometry that allows the optimization to simply reduce material.

4.5 FEM setup

From the generalized CAD-geometry, the forces and moments from every hundredth load steps obtained from Adams/Car are applied at the correct spots on the upright in Ansys Mechanical, whilst keeping some surfaces fixed. The fixed parts of the upright is colored with blue, with the different contact surfaces of the upright that are exposed to forces and moments shown in red according to figures 4.12 and 4.13.

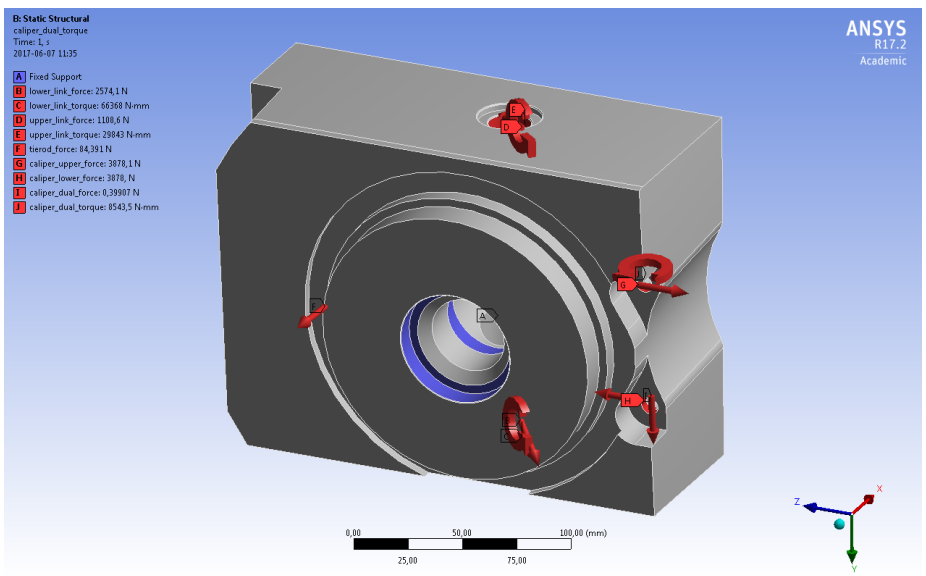

Figure 4.12: The fixed regions are shown in blue, with the surfaces with loads applied are shown as red.

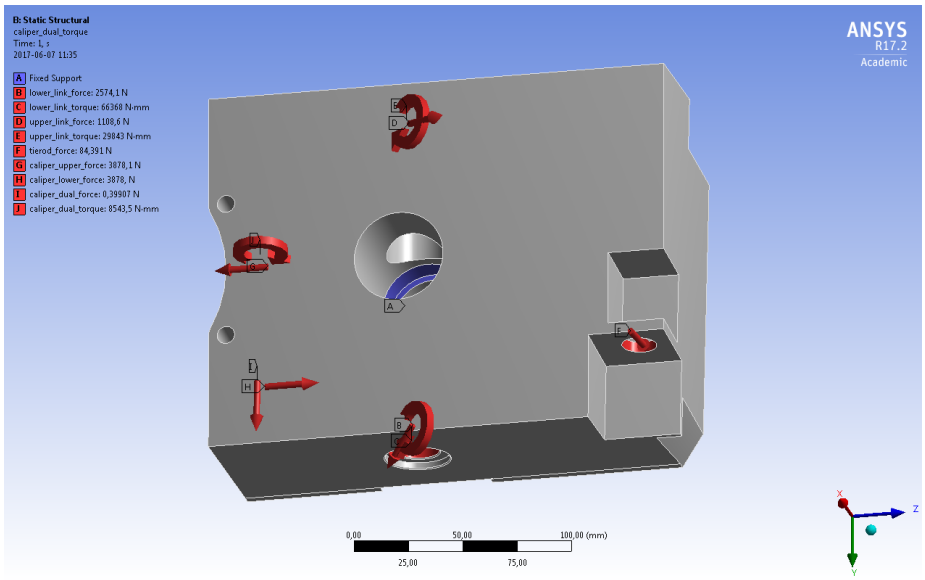

Figure 4.13: The fixed regions are shown in blue, with the surfaces with loads applied are shown as red, seen from behind.

The geometry is then meshed before a finite element analysis can be performed. The mesh is finer near the detailed features such as edges and holes, in order to capture the areas where sudden stress concentrations tend to arise[10]. This is tried with different meshes in order to find a mesh that is fine enough not to affect the results, but coarse enough not to require too much computing effort. The chosen mesh consists of tetrahedral elements after refinement to a finer mesh with 377 040 elements. Figures 4.14 and 4.15 shows the meshed upright.

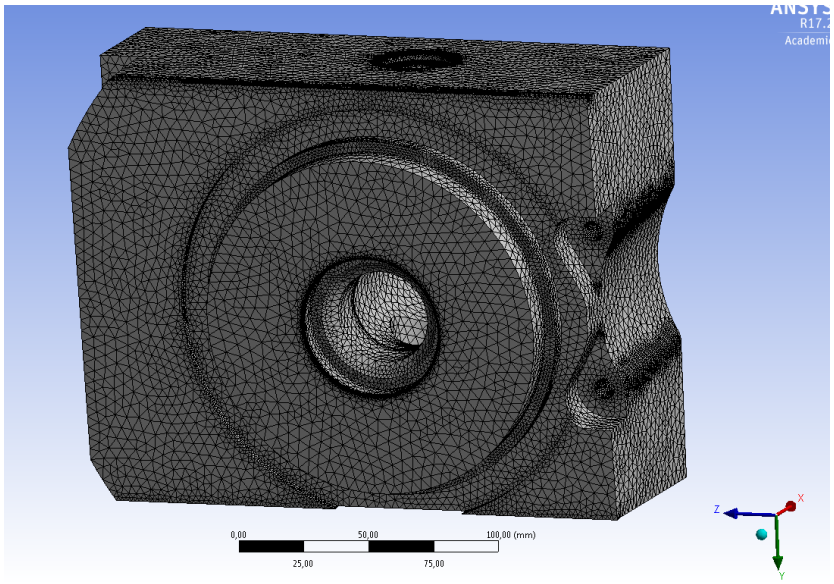

Figure 4.14: The meshed basic geometry for the optimization.

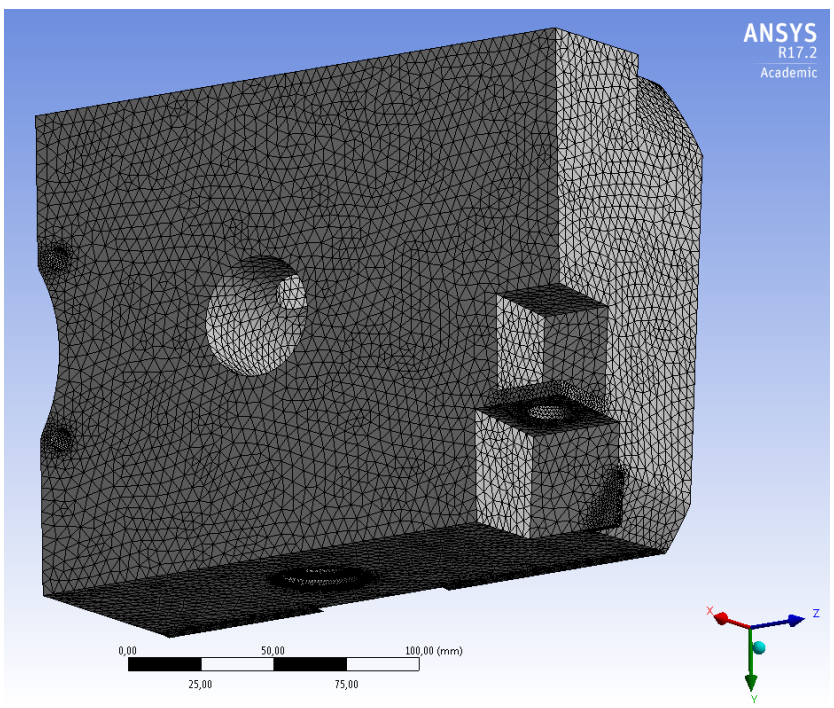

Figure 4.15: The meshed basic geometry for the optimization, seen from behind.

The material used for the initial fem analysis and the topology optimization is structural steel. The material parameters can be seen in table 4.5

Structural steel		
ρ	7850	kg/m^3
E	$2 \cdot 10^{11}$	Pa
ν	0.3	
σ_y	$2.5 \cdot 10^8$	Pa
σ_u	$4.6 \cdot 10^8$	Pa

Table 4.5: Material data for structural steel

4.6 Topology optimization

For the topology optimization stage the same loads and fixed support applied for the FEM analysis are used as boundary conditions for the optimization, with the difference that only one load step is applied, the chosen representative worst load case. The spots where the loads are applied have to be unchanged, since they are contiguous to other components that are connected with screws and bearings. In order to achieve this these spots need to be excluded from the optimization. Figures 4.16 and 4.17 show the excluded surfaces.

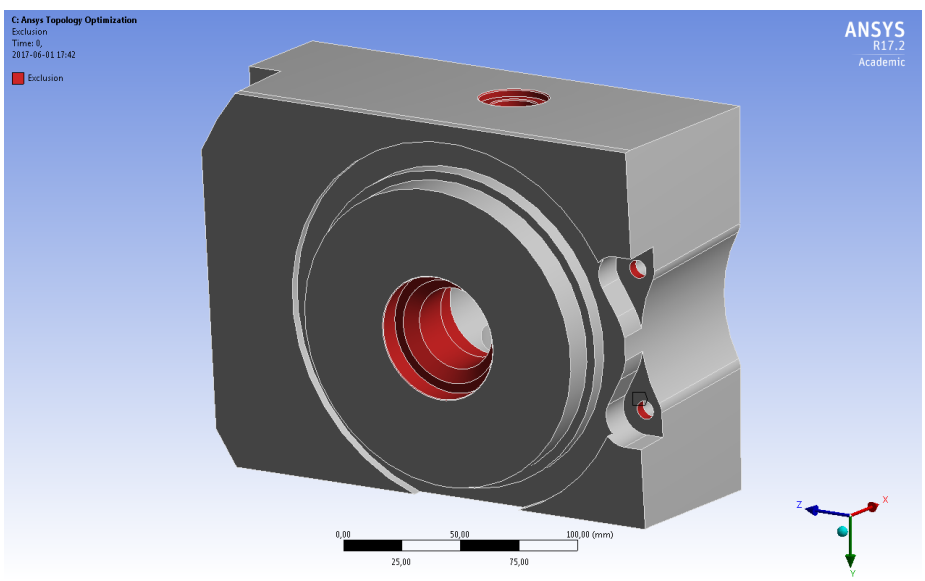

Figure 4.16: The basic excluded regions in the optimization marked in red.

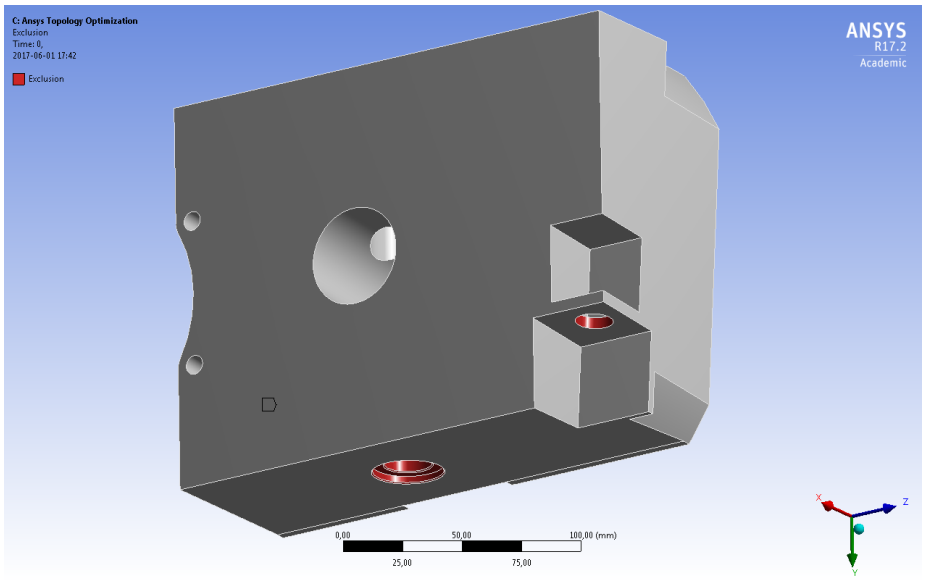

Figure 4.17: The basic excluded regions in the optimization marked in red, seen from behind.

The objective is set to minimize the mass, as was previously discussed. As constraint, the maximum stress value is limited to 125 MPa, which is half the tensile strength of the used steel material. Keeping this limit ensures that the material is kept within its linear elastic region. This ensures that a change of material to another linear elastic material will not alter results significantly regarding stress concentrations. However, a validation of the final geometry will be needed to be performed with the final material in order to ensure the final result will be as expected.

The topology optimization is then executed in Ansys Mechanical and an output geometry is obtained. The resulting geometry is not continuous and needs to be cleaned before validation.

4.7 Reverse engineering

SpaceClaim is used for cleaning up the geometry after the topology optimization, so called reverse engineering. SpaceClaim is the standard program used by Ansys for reverse engineering and features special functions for fixing messy geometries and smoothing them out. Finally the holes need to be recreated before the cleaned geometry can be used for validation.

4.8 Validation

Finally after obtaining a smooth final geometry, a validation can be performed in Ansys Mechanical. Just as for the initial FEM setup analysis on the generalized geometry, every hundredth load step from the Adams/Car simulations are used, since it has to be ensured that the final geometry can withstand the loads from all different drive cases at all different moments in time. If the final geometry can withstand all these load cases without unreasonably high stresses, it passes validation and can be approved for further refinement and eventually production. The mesh for the validation consists of 605 263 elements and can be seen in figures 4.18 and 4.19.

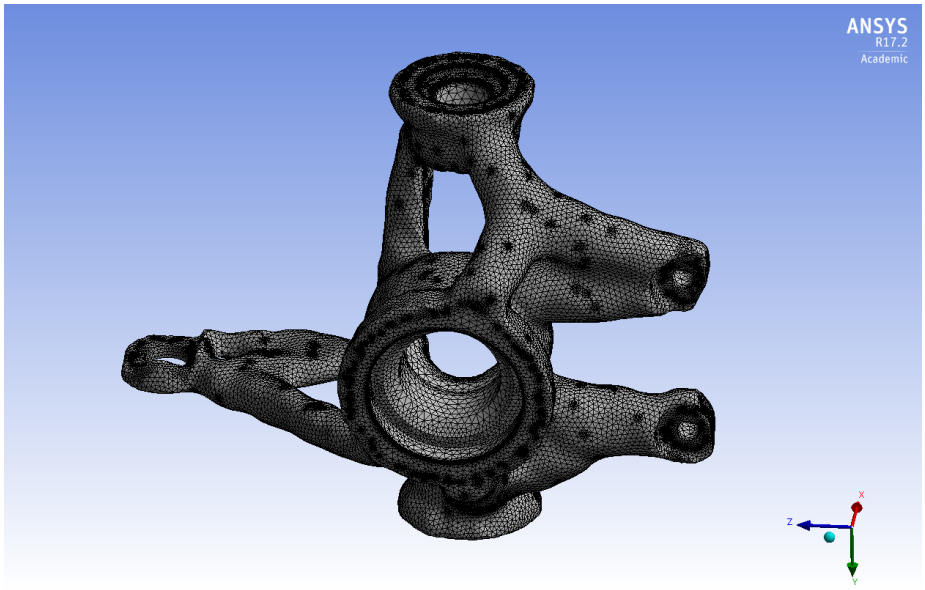

Figure 4.18: The mesh of the final geometry used for validation.

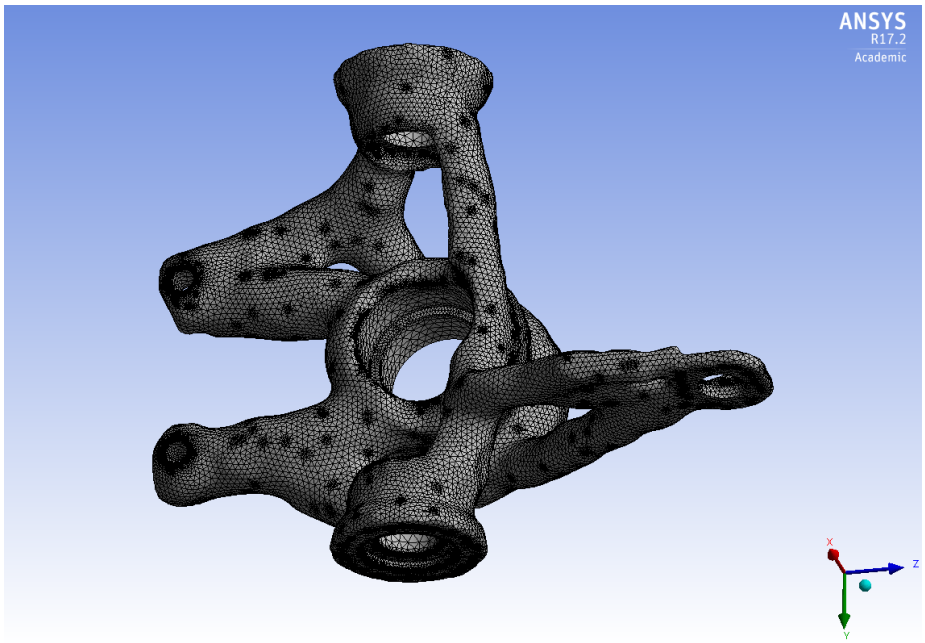

Figure 4.19: The mesh of the final geometry used for validation, seen from behind.

The material used for validation is an aluminum alloy (AlSi10Mg), and the material properties can be seen in table 4.6.

AlSi10Mg		
ρ	2700	kg/m^3
E	$6.4 \cdot 10^{10}$	Pa
ν	0.35	
σ_y	$2.27 \cdot 10^8$	Pa
σ_u	$3.97 \cdot 10^8$	Pa

Table 4.6: Material data for AlSi10Mg

Chapter 5

Results and discussion

5.1 Adams/Car

The resulting number of degrees of freedoms for the multibody system relative the chassis should be 7; one rotational for each wheel, one for suspension travel for each wheel, and finally one for the steering. The number of rigid bodies in the mechanism is calculated in table 5.1, and the number of joints and the number of degrees of freedom allowed are calculated in table 5.2.

Subsystem	B	RS	RW	S	FS	FW	Sum
Number of bodies	1	4	1	5	20	2	33

Table 5.1: Calculation of number of bodies

Subsystem	B	RS	RW	S	FS	FW	Sum	f_i	Sum
Fixed joints		0.5	0.5	1	7	1	10	0	0
Revolute joints	3	1.5		0.5	4		9	1	9
Translational joints	0.5			0.5			1	1	1
Hooke joints	1.5	1.5		2	3		8	2	16
Convel joints				1	1		2	2	4
Cylindrical joints	0.5	1		0.5	2		4	2	8
Spherical joints					6		6	3	18
Gears				1			1	5	5
						j:	41	$\sum f_i$:	61

Table 5.2: Calculation of degrees of freedom

Inserting the values from tables 5.1 and 5.2 into equation 3.3 yields:

$$M = 6(N - 1 - j) + \sum_{i=1}^{j} f_i = 6(33 - 1 - 41) + 61 = 7 \tag{5.1}$$

Which was to be expected. It shall, however, be noted that this is just an indication that the multibody system works as expected, it is by no means any guarantee. A more thorough analysis could have been made, but since the Greubler equation results in the expected value and since no odd behavior is observed in the Adams/Car simulations, there is no reason to suspect any problems[11].

The magnitudes of the resulting forces and moments from the Adams simulations can be seen in figures 5.1 and 5.2, with drive cases ordered as in table 5.3. For more detailed figures of the components of each force, see appendix C.

Number	Drive case
1	Acceleration
2	Braking
3	Constant radius cornering
4	ISO double lane change
5	Acceleration during cornering
6	Braking during cornering

Table 5.3: The way that the drive cases are ordered in the load diagrams.

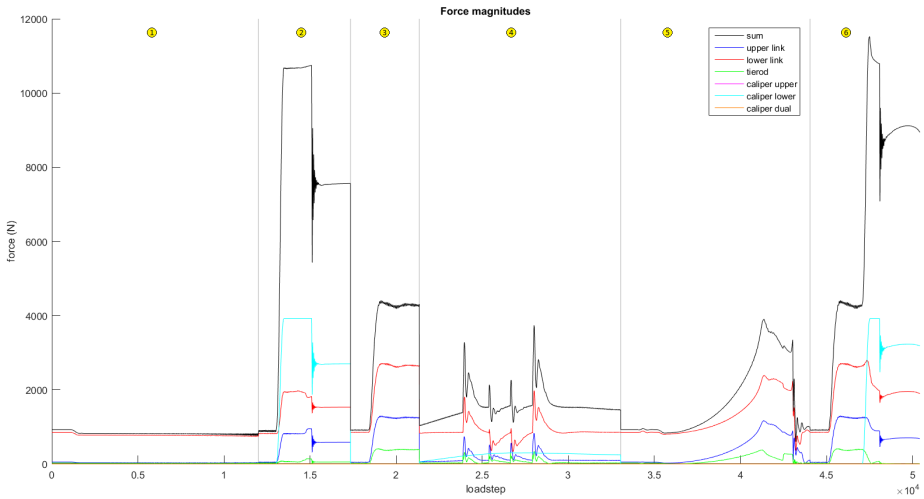

Figure 5.1: The magnitude of the different forces acting on the upright during different drive cases. Gray lines represent transition to the next drive case, ordered in the same way as presented in table 5.3.

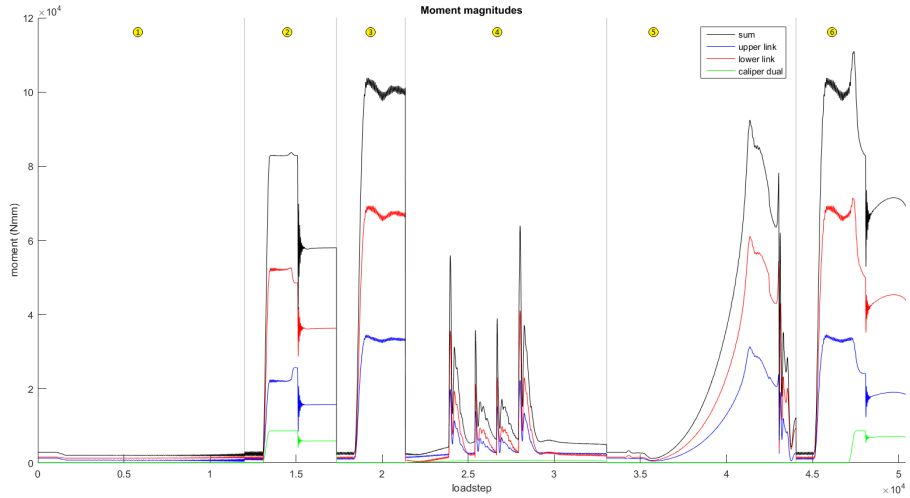

Figure 5.2: The magnitude of the different moments acting on the upright during different drive cases. Gray lines represent transition to the next drive case, ordered in the same way as presented in table 5.3.

From figures 5.1 and 5.2 it can be seen that the worst overall load case occurred when braking during cornering, more precisely at load step no 47 487. The loads from that case can be seen in tables 5.4 and 5.5.

Forces (N)	X-component	Y-component	Z-component
upper link	704.3981	121.0848	847.4183
lower link	-1332.302	1575.234	-1539.404
tierod	-83.91892	3.640149	8.141343
caliper upper	-14.80583973	1.294359866	-3878.104571
caliper lower	14.64947601	-1.280690197	3877.942673
caliper dual	0.03476737802	0.3975552408	0

Table 5.4: The forces acting on the upright in the chosen "worst load case" that is used as input for the topology optimization

Moments (Nmm)	X-component	Y-component	Z-component
upp_link_torque	-22958.69	125.1944	19065.34
low_link_torque	-50241.04	-113.967	43365.47
cal_rot_torque	-744.3091571	-8510.966976	0

Table 5.5: The moments acting on the upright in the chosen "worst load case" that is used as input for the topology optimization

These forces and moments were then used for the topology optimization.

It is not surprising that the worst case occurs when braking during cornering, since this is one of the cases where the tyres are the limiting factor, unlike plain acceleration and double lane change. Braking and cornering are on the limit each on their own, longitudinally and laterally respectively. Thus combined, the tyres are on the limit both longitudinally and laterally at the same time, implying that the overall case could be worse.

However it should be noted that this is only test cases on a plain road, with no bumps. It is likely that driving over bumps, such as pavements or pot holes, would yield worse scenarios. Therefore there should be a safety factor for the final upright.

5.2 Ansys

The results from the finite element analysis of the generalized geometry can be seen in figures 5.3, 5.4 and 5.5.

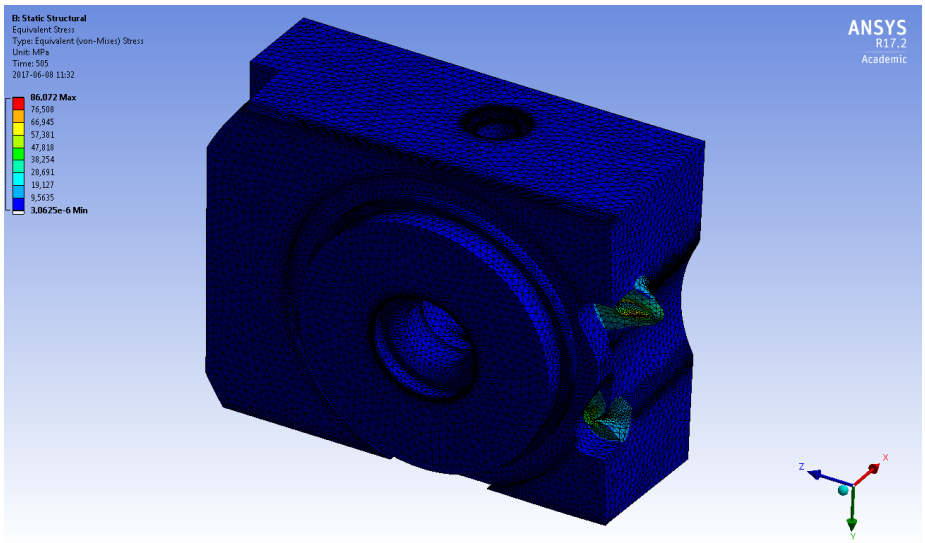

Figure 5.3: The result of the initial finite element analysis of the generalized geometry at the representative worst load step.

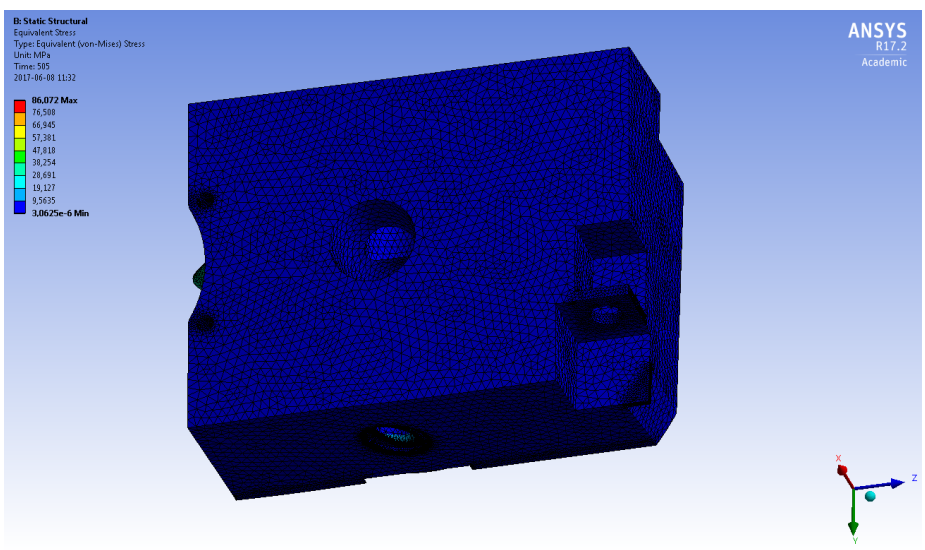

Figure 5.4: The result of the initial finite element analysis of the generalized geometry at the representative worst load step, seen from behind.

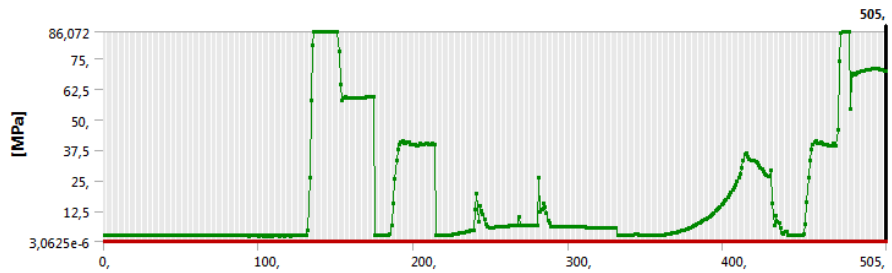

Figure 5.5: The maximum stress in the initial finite element analysis of the generalized geometry, plotted versus load step.

It is clear that this is unnecessarily large and heavy as the maximum von Mises-stress only reaches 86.072 MPa and much of the geometry has a stress of less than 10 MPa. It is obvious that much of the material is not necessary but can be removed.

The optimized geometry from the topology optimization is shown in figures 5.6 and 5.7. As can be seen, plenty of material has been removed, although the surfaces are very rough, likely due to the finite elements used in the optimization.

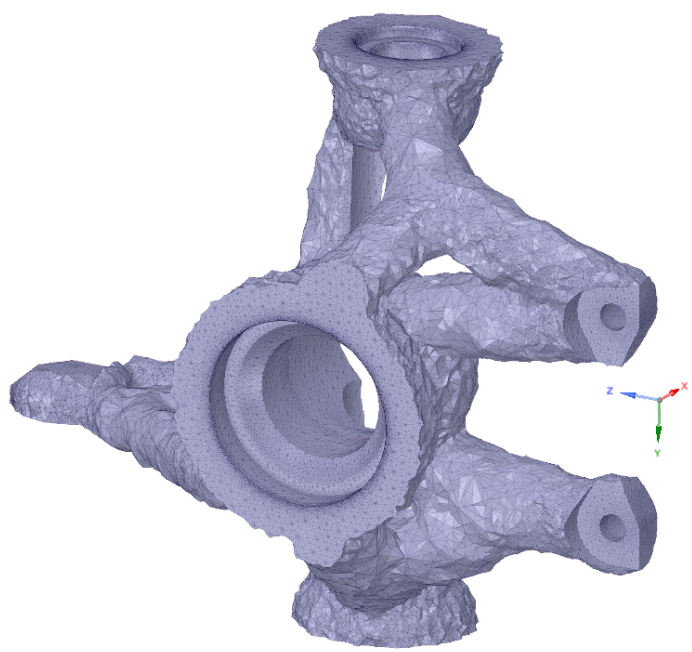

Figure 5.6: The output from the topology optimization.

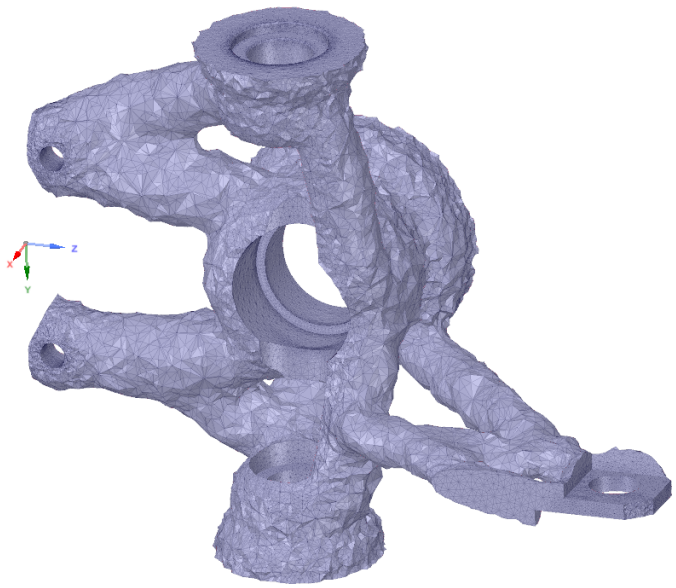

Figure 5.7: The output from the topology optimization, seen from behind.

Smaller elements would likely have helped making the resulting geometry smoother, although not likely to a satisfying level without impacting the simulation time heavily.

The geometry thus have to be refined and smoothed in SpaceClaim until a the geometry seen in figures 5.8 and 5.9 is obtained:

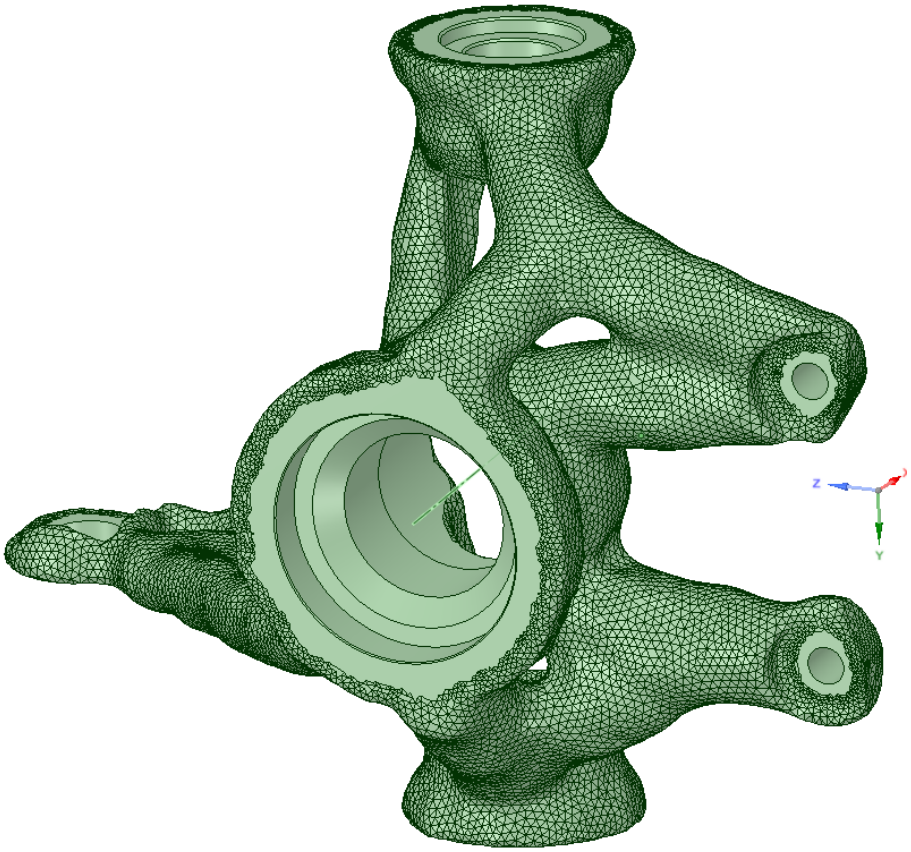

Figure 5.8: The optimized geometry smoothed in SpaceClaim.

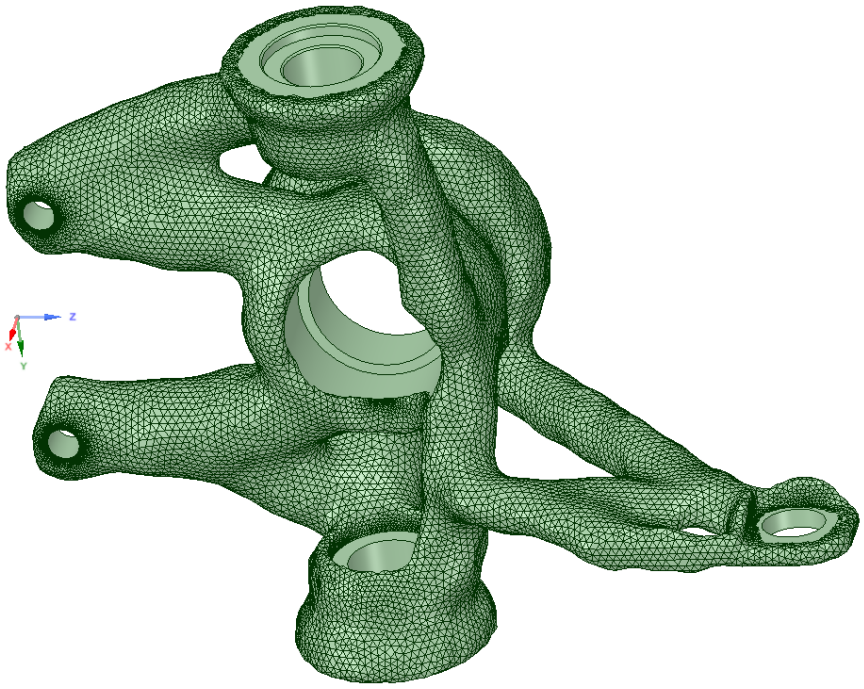

Figure 5.9: The optimized geometry smoothed in SpaceClaim, seen from behind.

Regarding the output of the optimization stage, there are some interesting details that are worth mentioning. As can be seen in figures 5.8 and 5.9 the excluded holes and surfaces are kept untouched and the interesting point is the fact that there are at least two link-arms that are extended from each hole except the hole in the centre of the upright. These link-arms work as a connection between each hole and they are tightened together in the centre-hole.

Using all load steps from figures 5.1 and 5.2, acting on the smoothed geometry seen in figure 5.8, the validation result can be seen in figures 5.10, 5.11 and 5.12

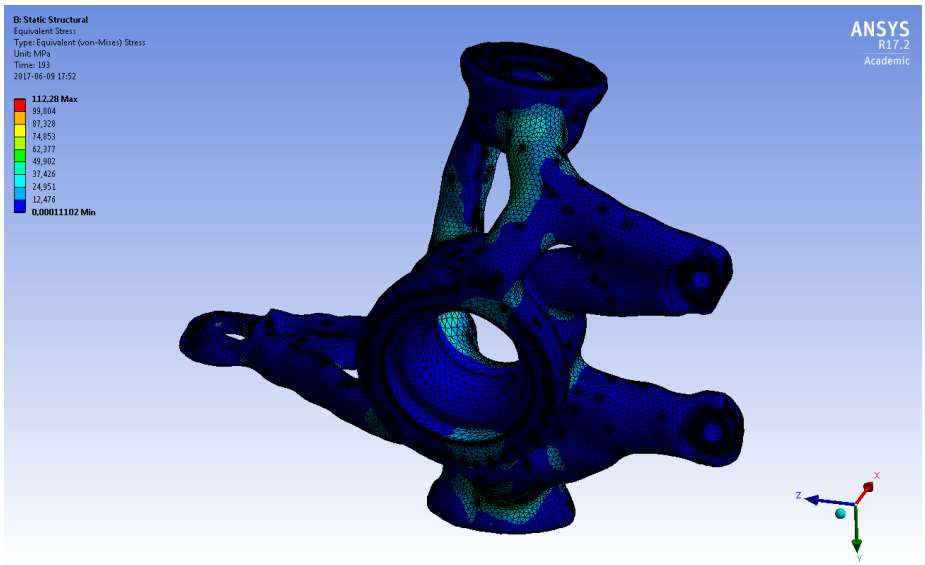

Figure 5.10: The result of the validation with maximum stresses.

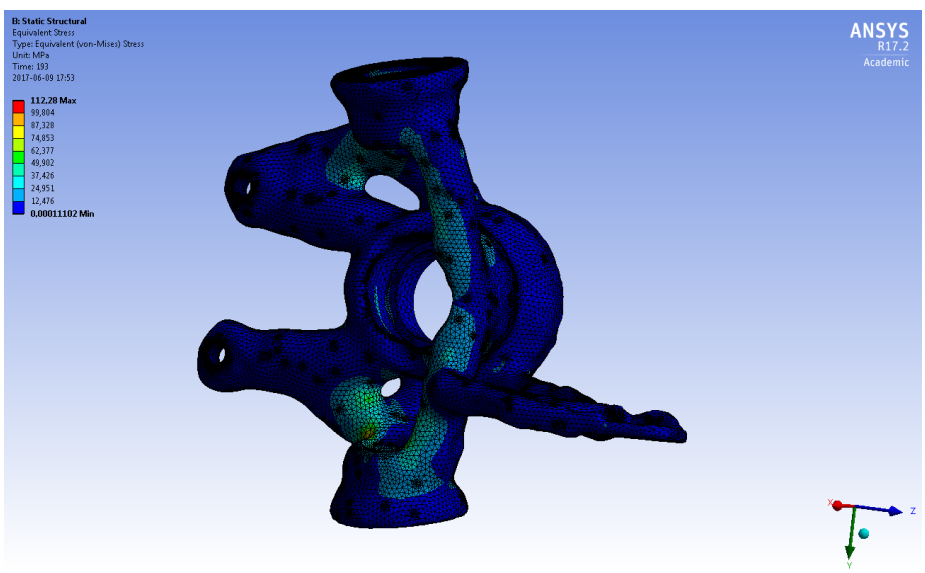

Figure 5.11: The result of the validation with maximum stresses, seen from behind.

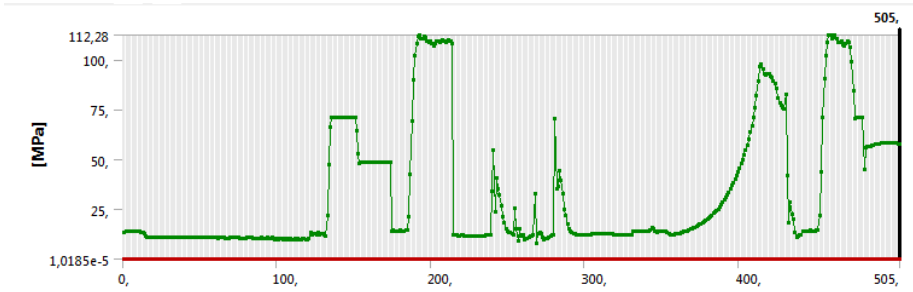

Figure 5.12: The maximum stress in the initial finite element analysis of the optimized geometry, plotted versus load step.

From the validation it becomes clear that the upright is able to withstand the loads from the input loads that were generated by the multibody simulations in Adams/Car. However there is no guarantee for it to resist worse loads cases that could occur when driving over bumps, such as pavements or potholes. As was previously discussed, this is due to the tyre model's inability to accurately represent the effects of sudden unevennesses. Further analyses regarding such events will need to be performed in order to ensure the reliability of the component.

Some notable simplifications of the finite element analysis are that neither the weight of the upright nor its acceleration is taken into account, and instead it is assumed to be fixed at the connections to the hub. Since the mass of the upright lies around 1 kg (apart from the generalized geometry which weights around 200 N) and thus weights about 10 N. The inertia forces from accelerations are normally less than that, around 0.8 times the weight at worst at maximal usage of the tyres. Compared to the forces which together reach 12000 N (figure 5.1) this can be seen as negligible.

Chapter 6

Summary of the results

A comparison of volume and mass between the old and the optimized upright was done and is shown in table 6.1. The generalized geometry is included for reference for the optimization on its own.

	V (dm^3)	ρ (kg/m^3)	m (kg)	σ_{max} (MPa)	SF
Previous upright assembly	0.4047	3652	1.478	N/A	N/A
Generalized upright geometry	2.932	7800	22.87	86.072	2.90
Optimized upright geometry	0.3461	2700	0.9345	112.28	2.02
Difference (%)	-14.5	-26.1	-36.8	N/A	N/A

Table 6.1: Comparison of the volumes and masses of the different versions of the upright.

The table shows that the mass has been reduced from 1.478 kg to 0.9345 kg, a reduction of 0.5435 kg or 36.8%. While this might be seen as insignificant, it is important to remember that this is a reduction of unsprung mass, which is far more critical than sprung mass regarding aspects such as ride quality[12].

Unfortunately a finite element analysis of the previous upright assembly was not performed since it would have required complicated modeling of the screws and contacts. Whilst this would have been achievable, it would have been very time consuming, and as it was never the main focus of this thesis to analyze the previous upright, it was not prioritized.

Since the chosen material were determined after the optimization, a substitution from structural steel to AlSi10Mg were only done for the optimized geometry. Validation of the stress concentrations on the optimized upright shows that the largest stresses are about 112 MPa, which is half of the yield strength for AlSi10Mg and thus a safety factor of just over 2 is obtained. This implies that

fatigue is unlikely to cause problems in the short term, although aluminum does not feature an endurance limit as other materials, such as steel, do[13]. A fatigue analysis was, however, not in the scoop of this thesis and therefore it is referred to as something that can be looked at in the future.

Chapter 7

Future work

The final geometry obtained in this thesis still consists of faceted surfaces, which could make manufacturing complicated depending on the manufacturing method and the product sub optimal. The next step would be to make the geometry surfaces smoother by adopting a mathematical algorithm which enables the faceted surfaces to be merged as one curved, described by splines.

Since the main task of this master thesis is to come up with one single upright, the manufacturing was not of vital interest. For that reason there are no analysis of the manufacture method or manufacture cost present in this work and whether it is optimal when it comes to mass producing a series of uprights. In order to do this the design-to-cost of the upright has to be analyzed and an optimal geometry for a minimal price has to be developed since the only optimization condition was minimization of the mass with a constraint that limited the stresses to a maximum value. As soon as an optimal design has been determined an appropriate manufacturing method has to be chosen. This could be done in a separate master thesis in a more extended way.

A more detailed finite element analysis of the upright, by introducing the bodies with which the upright is in contact, such as ball bearings, brake caliper and A-arms, ought to be considered in the future since this would yield in a more representative result. Additionally, a fatigue analysis would be an interesting addition to this thesis.

It would also be interesting to see the effects of flexible bodies in Adams/Car to yield a more representative model. The effects of compliance in the upright, as well as the other components, could potentially play a significant role in affecting the handling of the vehicle.

Additionally, sensitivity analyses would be interesting to carry out, especially on tyre parameters, in order to see how big effect they have on the reaction loads and further on to the optimization.

The Adams/Car model created could also be used for analyzing the handling of the vehicle for tuning of the suspension parameters in a future study.

Bibliography

(1) M. Boxwell, *Electric Car History*, https://web.archive.org/web/20140105043545/http://www.owningelectriccar.com/electric-car-history.html (visited on 2017-06-19).

(2) Tesla, *About Tesla*, https://www.tesla.com/about (visited on 2017-06-07).

(3) M. Graham, *Engineering a 3 Wheel Vehicle Chassis*, https://engineerdog.com/2015/09/09/engineering-a-3-wheel-vehicle-chassis/ (visited on 2017-06-19).

(4) J. L. Meriam and L. G. Kraige, *Engineering Mechanics - Dynamics*, Wiley, 2013.

(5) V. Smutný, *Robotics: Kinematics - Introduction*, http://cmp.felk.cvut.cz/cmp/courses/ROB/roblec/kinematika-noteeng (visited on 2017-06-07).

(6) Adams, *Adams/Car manual*, https://simcompanion.mscsoftware.com/infocenter/index?page=content&id=DOC11180& (visited on 2017-06-07).

(7) Adams, *Adams/Tire manual*, https://simcompanion.mscsoftware.com/infocenter/index?page=content&id=DOC11199&actp=RSS (visited on 2017-06-07).

(8) N. Saabye Ottosen and M. Ristinmaa, *The Mechanics of Constitutive Modeling*, Elsevier Science, 2005.

(9) Edy, *Pacejka '94 parameters explalined - a comprehensive guide*, http://www.edy.es/dev/docs/pacejka-94-parameters-explained-a-comprehensive-guide/ (visited on 2017-06-09).

(10) I. Kokcharov, *Structural Integrity Analysis - Stress Concentration*, http://www.kokch.kts.ru/me/t1/SIA_1_Stress_Concentration.pdf (visited on 2017-06-19).

(11) M. Blundell and D. Harty, *The Multibody Systems Approach to Vehicle Dynamics*, Elsevier, 2004.

(12) M. Miwa, Y. Kawasaki and A. Yoshimura, *Influence of vehicle unsprung-mass on dynamic wheel load*, https://www.witpress.com/Secure/elibrary/papers/CR08/CR08069FU1.pdf (visited on 2017-06-09).

(13) F. C. Campbell, *Elements of Metallurgy and Engineering Alloys*, ASM International, 2008.

Appendix A

Lists of joints

Rear suspension:			
Joint name	Parts		Type of joint
damper_joint	forward damper half	rearward damper half	Cylindrical
damper_to_frame	forward damper half	body mount (body)	Hooke
arms_to_frame	swing arm	body mount (body)	Revolute
damper_to_arms	swing arm	rearward damper half	Hooke
axle_joint	swing arm	rim	Revolute

Table A.1: List of joints in the rear suspension subsystem

Rear wheel:			
Joint name	Parts		Type of joint
wheel_to_spindle	rear wheel	rim (rear suspension)	Fixed

Table A.2: List of joints in the rear wheel subsystem

Steering:			
Joint name	Parts		Type of joint
steering_input_shaft	pinion shaft	rack housing (body)	Revolute
steering_column_to_body	steering column	column support (body)	Cylindrical
steering_wheel	steering wheel	steering column	Fixed
rack_to_rackhousing	rack	rack housing (body)	Translational
intermediate_shaftinput	intermediate shaft	pinion shaft	Hooke
column_intermediate	steering column	intermediate shaft	Hooke

Table A.3: List of joints in the steering subsystem

Front suspension:			
Joint name	Parts		Type of joint
caliper_to_upright	brake caliper	upright	Fixed
upright_lower_link	upper upright link	upright	Fixed
upright_upper_link	lower upright link	upright	Fixed
spindle_upright	hub	upright	Revolute
lwr_strut	lower damper half	lower A-arm	Hooke
uca	upper A-arm	body mount (body)	Revolute
lwr_upr_strut	lower damper half	upper damper half	Cylindrical
uca_balljoint	upper A-arm	upper upright link	Spherical
top_mount	upper damper half	body mount (body)	Hooke
tierod_inner	tierod	rack	Convel
tierod_outer	tierod	upright	Spherical
lca_balljoint	lower upright link	lower A-arm	Spherical
lca	lower A-arm	body mount (body)	Revolute

Table A.4: List of joints in the front suspension subsystem

Front wheels:			
Joint name	Parts		Type of joint
wheel_to_spindle	front wheel	hub (front suspension)	Fixed

Table A.5: List of joints in the front wheels subsystem

Appendix B

Tyre files

ecoist_front_tire.tir:

```
$----------------------------------------------------------------------MDI_HEADER
[MDI_HEADER]
 FILE_TYPE     =  'tir'
 FILE_VERSION  =  3.0
 FILE_FORMAT   =  'ASCII'
(COMMENTS)
{comment_string}
'Tire      - XXXXXX'
'Pressure  - XXXXXX'
'Test Date - XXXXXX'
'Test tire'
$--------------------------------------------------------------------------units
[UNITS]
 LENGTH              = 'mm'
 FORCE               = 'newton'
 ANGLE               = 'radian'
 MASS                = 'kg'
 TIME                = 'sec'
$--------------------------------------------------------------------------model
[MODEL]
! use mode    1   2   3   4    11   12   13   14
! ---------------------------------------------------------------------------
! smoothing           X   X              X    X
! combined        X       X         X         X
! transient                     X    X    X    X
!
 PROPERTY_FILE_FORMAT    = 'PAC89'
 USE_MODE                = 4.0
! 3D contact can be switched on by deleting the comment ! character
! When no further coefficients are specified, default values will be taken
!CONTACT_MODEL            = '3D_ENVELOPING'
$----------------------------------------------------------------------dimensions
[DIMENSION]
 UNLOADED_RADIUS         = 259.5
```

```
 WIDTH                   = 62.4
 ASPECT_RATIO            = 1.34
$-----------------------------------------------------------------------vertical
[PARAMETER]
 VERTICAL_STIFFNESS      = 310.0
 VERTICAL_DAMPING        = 3.1
 LATERAL_STIFFNESS       = 190.0
 ROLLING_RESISTANCE  = 0.0
$-----------------------------------------------------------------------lateral
[LATERAL_COEFFICIENTS]
 a0  =  1.40
 a1  =  0.0
 a2  =  800.0
 a3  =  1100.0
 a4  =  10.0
 a5  =  0.0
 a6  =  0.0
 a7  =  -2.0
 a8  =  0.0
 a9  =  0.0
 a10 =  0.0
 a11 =  0.0
 a12 =  0.0
 a13 =  0.0
$-----------------------------------------------------------------longitudinal
[LONGITUDINAL_COEFFICIENTS]
 b0  =  1.50
 b1  =  0.0
 b2  =  800.0
 b3  =  0.0
 b4  =  300.0
 b5  =  0.0
 b6  =  0.0
 b7  =  0.0
 b8  =  -2.0
 b9  =  0.0
 b10 =  0.0
$-----------------------------------------------------------------------aligning
[ALIGNING_COEFFICIENTS]
 c0  =  2.34000
 c1  =  1.4950
 c2  =  6.416654
 c3  = -3.57403
 c4  = -0.087737
 c5  =  0.098410
 c6  =  0.0027699
 c7  = -0.0001151
 c8  =  0.1000
 c9  = -1.33329
 c10 =  0.025501
 c11 = -0.02357
 c12 =  0.03027
 c13 = -0.0647
 c14 =  0.0211329
 c15 =  0.89469
 c16 = -0.099443
 c17 = -3.336941
```

```
$-----------------------------------------------------------------------shape
[SHAPE]
{radial width}
 1.0    0.0
 1.0    0.2
 1.0    0.4
 1.0    0.5
 1.0    0.6
 1.0    0.7
 1.0    0.8
 1.0    0.85
 1.0    0.9
 0.9    1.0
```

ecoist_rear_tire.tir:

```
$-------------------------------------------------------------------MDI_HEADER
[MDI_HEADER]
 FILE_TYPE     =  'tir'
 FILE_VERSION  =  3.0
 FILE_FORMAT   =  'ASCII'
(COMMENTS)
{comment_string}
'Tire      - XXXXXX'
'Pressure  - XXXXXX'
'Test Date - XXXXXX'
'Test tire'
$----------------------------------------------------------------------------units
[UNITS]
 LENGTH              = 'mm'
 FORCE               = 'newton'
 ANGLE               = 'radian'
 MASS                = 'kg'
 TIME                = 'sec'
$----------------------------------------------------------------------------model
[MODEL]
! use mode    1   2   3   4    11   12   13   14
! ---------------------------------------------------------------------------
! smoothing           X   X              X    X
! combined        X       X         X         X
! transient                   X    X    X    X
!
 PROPERTY_FILE_FORMAT    = 'PAC89'
 USE_MODE                = 4.0
! 3D contact can be switched on by deleting the comment ! character
! When no further coefficients are specified, default values will be taken
!CONTACT_MODEL            = '3D_ENVELOPING'
$-------------------------------------------------------------------dimensions
[DIMENSION]
 UNLOADED_RADIUS         = 305.0
 WIDTH                   = 105.0
 ASPECT_RATIO            = 0.95
$-------------------------------------------------------------------vertical
[PARAMETER]
 VERTICAL_STIFFNESS      = 310.0
 VERTICAL_DAMPING        = 3.1
 LATERAL_STIFFNESS       = 190.0
 ROLLING_RESISTANCE  = 0.0
$-------------------------------------------------------------------lateral
[LATERAL_COEFFICIENTS]
 a0  =  1.40
 a1  =  0.0
 a2  =  800.0
 a3  =  1100.0
 a4  =  10.0
 a5  =  0.0
 a6  =  0.0
 a7  =  -2.0
 a8  =  0.0
 a9  =  0.0
```

```
 a10 =  0.0
 a11 =  0.0
 a12 =  0.0
 a13 =  0.0
$-------------------------------------------------------------------longitudinal
[LONGITUDINAL_COEFFICIENTS]
 b0  =  1.50
 b1  =  0.0
 b2  =  800.0
 b3  =  0.0
 b4  =  300.0
 b5  =  0.0
 b6  =  0.0
 b7  =  0.0
 b8  =  -2.0
 b9  =  0.0
 b10 =  0.0
$--------------------------------------------------------------------aligning
[ALIGNING_COEFFICIENTS]
 c0  =  2.34000
 c1  =  1.4950
 c2  =  6.416654
 c3  = -3.57403
 c4  = -0.087737
 c5  =  0.098410
 c6  =  0.0027699
 c7  = -0.0001151
 c8  =  0.1000
 c9  = -1.33329
 c10 =  0.025501
 c11 = -0.02357
 c12 =  0.03027
 c13 = -0.0647
 c14 =  0.0211329
 c15 =  0.89469
 c16 = -0.099443
 c17 = -3.336941
$-----------------------------------------------------------------------------shape
[SHAPE]
{radial width}
 1.0    0.0
 1.0    0.2
 1.0    0.4
 1.0    0.5
 1.0    0.6
 1.0    0.7
 1.0    0.8
 1.0    0.85
 1.0    0.9
 0.9    1.0
```

Appendix C

Load curves

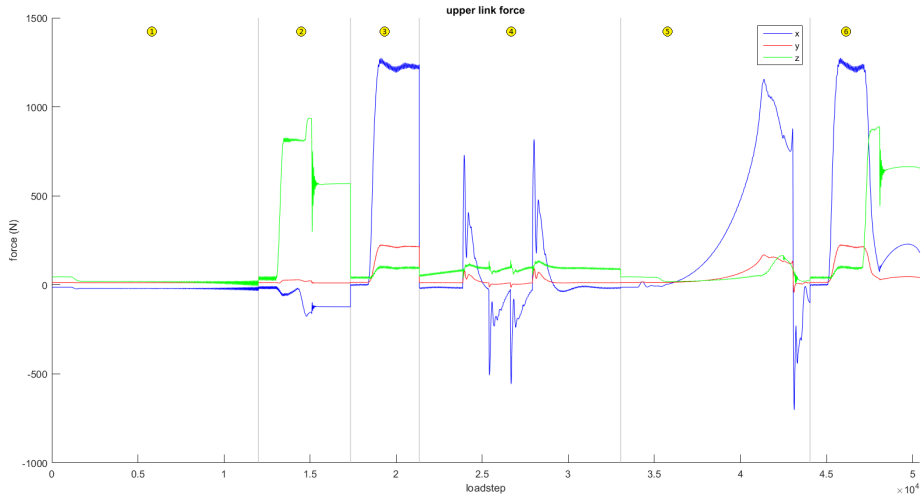

Figure C.1: The x, y and z components of the upper link force for each load step. Gray lines represent transition to the next drive case, ordered in the same way as presented in table 5.3.

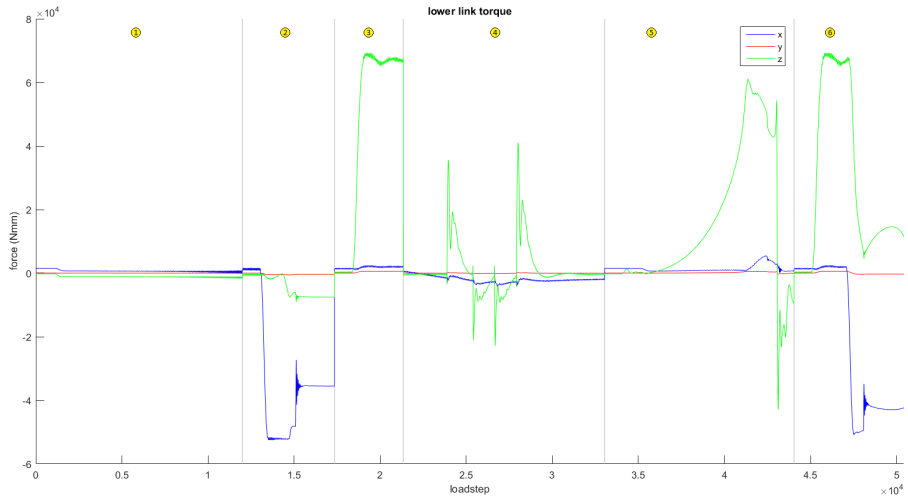

Figure C.2: The x, y and z components of the lower link force for each load step. Gray lines represent transition to the next drive case, ordered in the same way as presented in table 5.3.

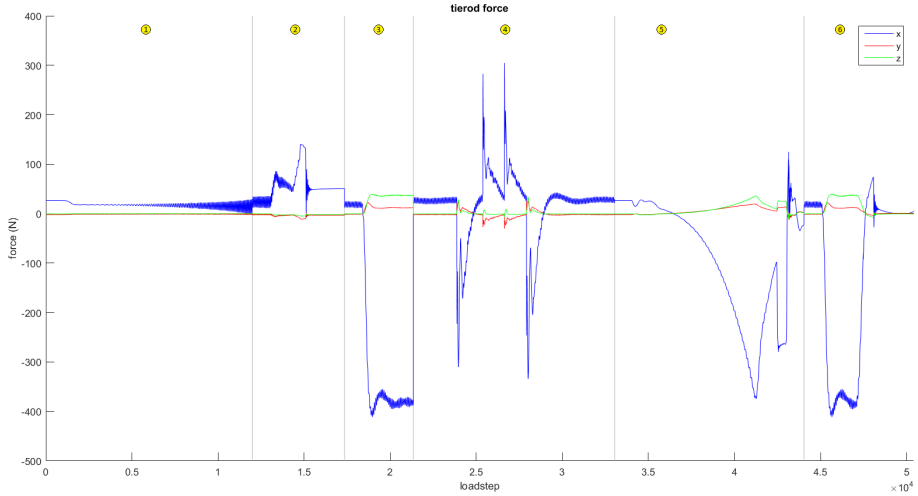

Figure C.3: The x, y and z components of the tierod force for each load step. Gray lines represent transition to the next drive case, ordered in the same way as presented in table 5.3.

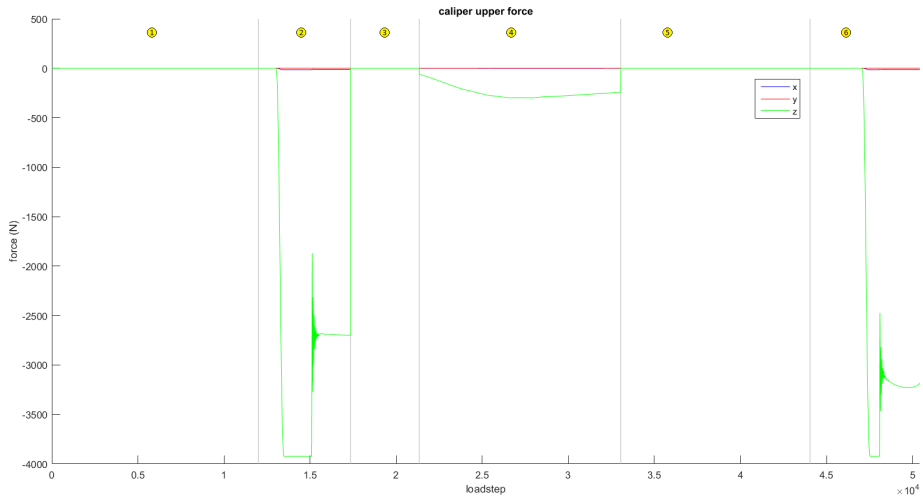

Figure C.4: The x, y and z components of the caliper upper force for each load step. Gray lines represent transition to the next drive case, ordered in the same way as presented in table 5.3.

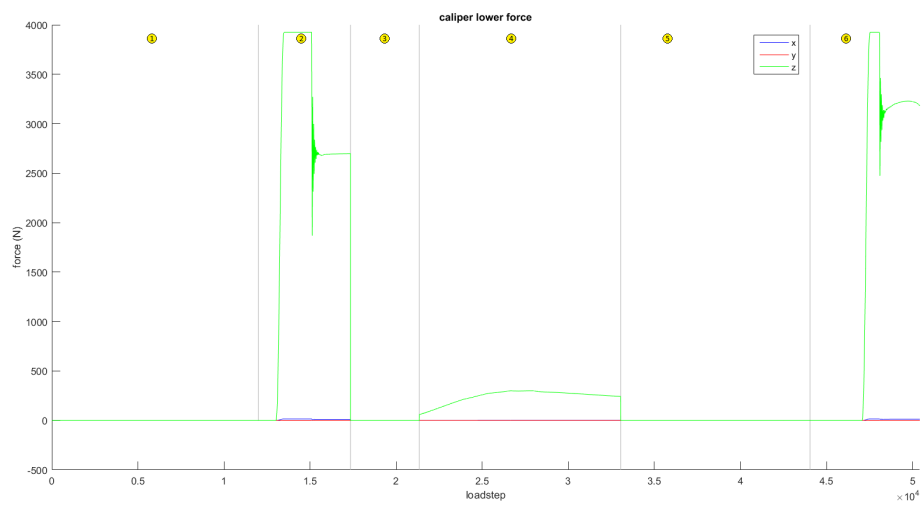

Figure C.5: The x, y and z components of the caliper lower force for each load step. Gray lines represent transition to the next drive case, ordered in the same way as presented in table 5.3.

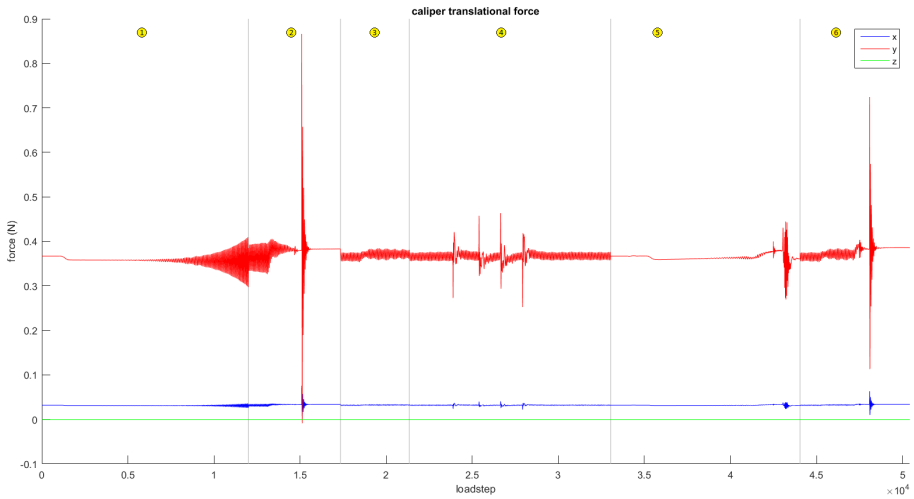

Figure C.6: The x, y and z components of the caliper translational force for each load step. Gray lines represent transition to the next drive case, ordered in the same way as presented in table 5.3.

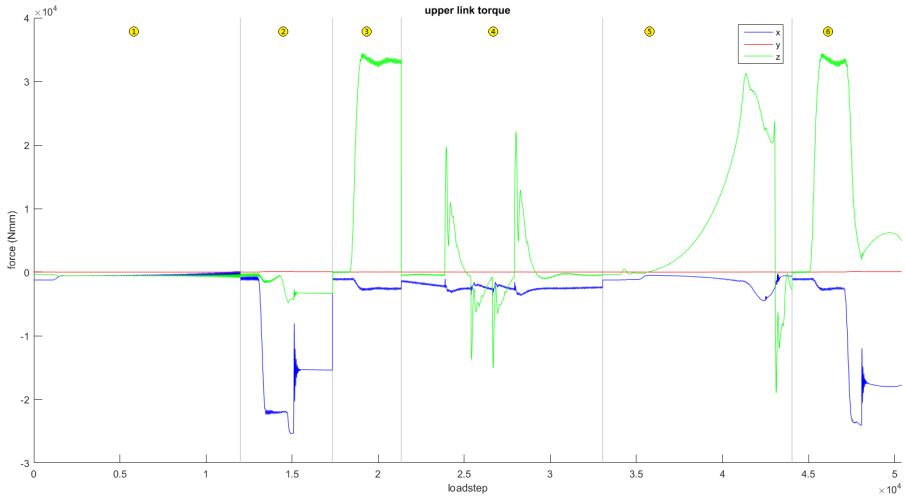

Figure C.7: The x, y and z components of the upper link torque for each load step. Gray lines represent transition to the next drive case, ordered in the same way as presented in table 5.3.

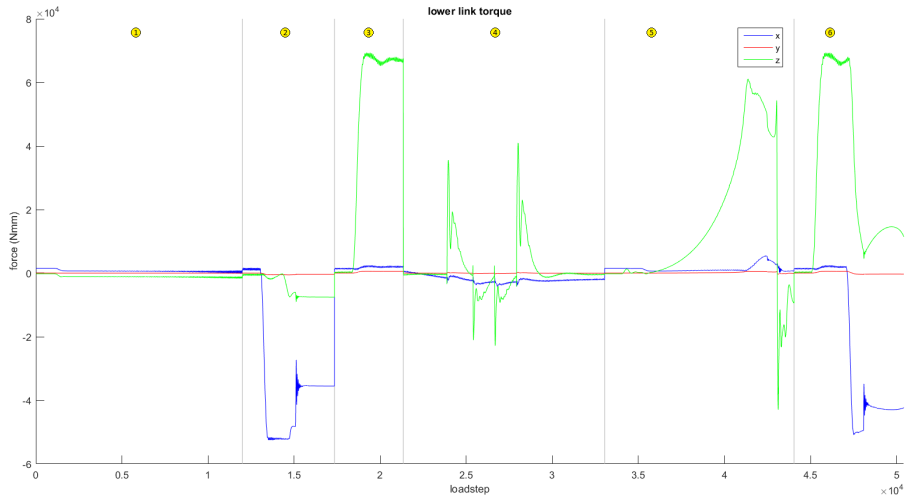

Figure C.8: The x, y and z components of the lower link torque for each load step. Gray lines represent transition to the next drive case, ordered in the same way as presented in table 5.3.

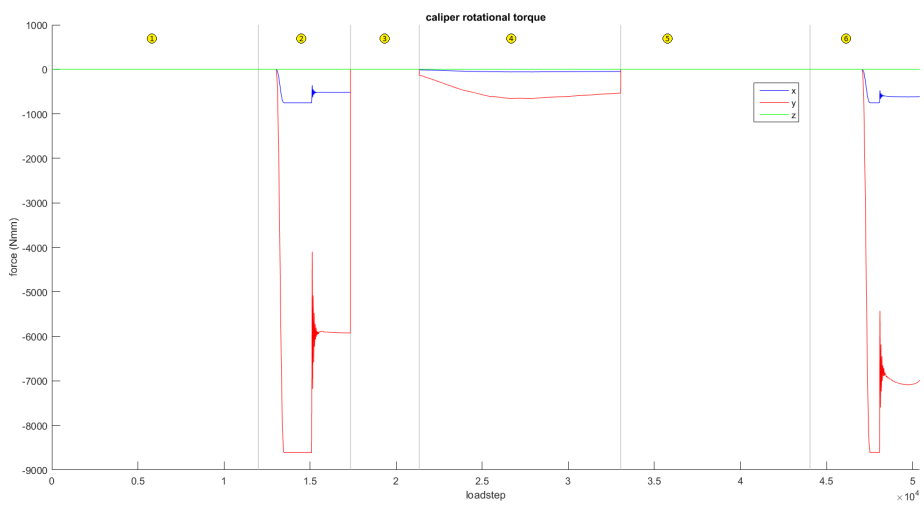

Figure C.9: The x, y and z components of the caliper rotational torque for each load step. Gray lines represent transition to the next drive case, ordered in the same way as presented in table 5.3.

Appendix D

Matlab code - Powertrain

```
clear
close all
clc

gearing = 4.54;
T_max_motor = 47;                          %Nm
T_max_wheel = T_max_motor*gearing;         %Nm
n_max_motor = 4000;                        %rpm
n_max_wheel = n_max_motor/gearing;         %rpm
omega_max_motor = n_max_motor*2*pi/60;     %rad/s
omega_max_wheel = n_max_wheel*2*pi/60;     %rad/s
P_max_motor = T_max_motor*omega_max_motor  %W
P_max_wheel = T_max_wheel*omega_max_wheel  %W
```

Appendix E

Matlab code - Worst load case

```
clear
close all
clc

acceleration_caliper;
acceleration_lower_link;
acceleration_tierod;
acceleration_upper_link;
braking_caliper;
braking_lower_link;
braking_tierod;
braking_upper_link;
bump_caliper;
bump_lower_link;
bump_tierod;
bump_upper_link;
corner_acc_caliper;
corner_acc_lower_link;
corner_acc_tierod;
corner_acc_upper_link;
corner_brake_caliper;
corner_brake_lower_link;
corner_brake_tierod;
corner_brake_upper_link;
cornering_caliper;
cornering_lower_link;
cornering_tierod;
cornering_upper_link;
lanechange_caliper;
lanechange_lower_link;
lanechange_tierod;
lanechange_upper_link;
pothole_caliper;
```

```
pothole_lower_link;
pothole_tierod;
pothole_upper_link;

first = 1001;

limit = [];
limit = [limit;length(acc_upp_link(first:end,2:5))];
limit = [limit;limit(1)+length(brake_upp_link(first:end,2:5))];
limit = [limit;limit(2)+length(corner_upp_link(first:end,2:5))];
limit = [limit;limit(3)+length(ilc_upp_link(first:end,2:5))];
limit = [limit;limit(4)+length(coracc_upp_link(first:end,2:5))];



upp_link_force = [acc_upp_link(first:end,2:5)
    brake_upp_link(first:end,2:5)
    corner_upp_link(first:end,2:5)
    ilc_upp_link(first:end,2:5)
    coracc_upp_link(first:end,2:5)
    corbra_upp_link(first:end,2:5)
    ];
for i=1:length(upp_link_force)
    upp_link_force(i,1) = norm(upp_link_force(i,2:4));
end

upp_link_torque = [acc_upp_link(first:end,6:9)
    brake_upp_link(first:end,6:9)
    corner_upp_link(first:end,6:9)
    ilc_upp_link(first:end,6:9)
    coracc_upp_link(first:end,6:9)
    corbra_upp_link(first:end,6:9)
    ];
for i=1:length(upp_link_torque)
    upp_link_torque(i,1) = norm(upp_link_torque(i,2:4));
end



low_link_force = [acc_low_link(first:end,2:5)
    brake_low_link(first:end,2:5)
    corner_low_link(first:end,2:5)
    ilc_low_link(first:end,2:5)
    coracc_low_link(first:end,2:5)
    corbra_low_link(first:end,2:5)
    ];
for i=1:length(low_link_force)
    low_link_force(i,1) = norm(low_link_force(i,2:4));
end

low_link_torque = [acc_low_link(first:end,6:9)
    brake_low_link(first:end,6:9)
    corner_low_link(first:end,6:9)
    ilc_low_link(first:end,6:9)
    coracc_low_link(first:end,6:9)
    corbra_low_link(first:end,6:9)
    ];
```

```
for i=1:length(low_link_torque)
    low_link_torque(i,1) = norm(low_link_torque(i,2:4));
end



tie_force = [acc_tie(first:end,2:5)
    brake_tie(first:end,2:5)
    corner_tie(first:end,2:5)
    ilc_tie(first:end,2:5)
    coracc_tie(first:end,2:5)
    corbra_tie(first:end,2:5)
    ];
for i=1:length(tie_force)
    tie_force(i,1) = norm(tie_force(i,2:4));
end



cal_force = [acc_cal(first:end,2:5)
    brake_cal(first:end,2:5)
    corner_cal(first:end,2:5)
    ilc_cal(first:end,2:5)
    coracc_cal(first:end,2:5)
    corbra_cal(first:end,2:5)
    ];
for i=1:length(cal_force)
    cal_force(i,1) = norm(cal_force(i,2:4));
end

cal_torque = [acc_cal(first:end,6:9)
    brake_cal(first:end,6:9)
    corner_cal(first:end,6:9)
    ilc_cal(first:end,6:9)
    coracc_cal(first:end,6:9)
    corbra_cal(first:end,6:9)
    ];
for i=1:length(cal_torque)
    cal_torque(i,1) = norm(cal_torque(i,2:4));
end

%Recalculating fixed caliper joint to the tho points

F_x = cal_force(:,2);
F_y = cal_force(:,3);
F_z = cal_force(:,4);

T_x = cal_torque(:,2);
T_y = cal_torque(:,3);
T_z = cal_torque(:,4);

h = 63.5;

R_ux = F_x/2 + T_z/h;
R_lx = F_x/2 - T_z/h;
R_uz = F_z/2 - T_x/h;
R_lz = F_z/2 + T_x/h;
```

```
R_y = F_y;
M_y = T_y;

a1 = [57.88;-5.06;0];
a2 = [6.97;79.70;0];
a3 = [0;0;15.75];

a1 = a1/norm(a1);
a2 = a2/norm(a2);
a3 = a3/norm(a3);

A = [a1,a2,a3];

cal_upp_force = zeros(length(M_y),4);
cal_low_force = zeros(length(M_y),4);
cal_trans_force = zeros(length(M_y),4);
cal_rot_torque = zeros(length(M_y),4);

for i=1:length(M_y)
    cal_upp_force(i,2:4) = (A*[R_ux(i);0;R_uz(i)])';
    cal_low_force(i,2:4) = (A*[R_lx(i);0;R_lz(i)])';
    cal_trans_force(i,2:4) = (A*[0;R_y(i);0])';
    cal_rot_torque(i,2:4) = (A*[0;M_y(i);0])';

    cal_upp_force(i,1) = norm(cal_upp_force(i,2:4));
    cal_low_force(i,1) = norm(cal_low_force(i,2:4));
    cal_trans_force(i,1) = norm(cal_trans_force(i,2:4));
    cal_rot_torque(i,1) = norm(cal_rot_torque(i,2:4));
end


sum_force_mag = upp_link_force(:,1) + low_link_force(:,1) + tie_force(:,1) +
cal_upp_force(:,1) + cal_low_force(:,1) + cal_trans_force(:,1);
sum_torque_mag = upp_link_torque(:,1) + low_link_torque(:,1) + cal_rot_torque(:,1);

gray = [0.7 0.7 0.7];
orange = [1 0.5 0];



% Code for plotting figures

figure
title('Force magnitudes')
hold on
xlabel('loadstep')
ylabel('force (N)')
plot(sum_force_mag,'w')
plot([limit(1),limit(1)],ylim,'Color',gray)
plot([limit(2),limit(2)],ylim,'Color',gray)
plot([limit(3),limit(3)],ylim,'Color',gray)
plot([limit(4),limit(4)],ylim,'Color',gray)
plot([limit(5),limit(5)],ylim,'Color',gray)
p1 = plot(upp_link_force(:,1),'b');
p2 = plot(low_link_force(:,1),'r');
p3 = plot(tie_force(:,1),'g');
p4 = plot(cal_upp_force(:,1),'m');
```

```
p5 = plot(cal_low_force(:,1),'c');
p6 = plot(cal_trans_force(:,1),'Color',orange);
p0 = plot(sum_force_mag,'k');
legend([p0,p1,p2,p3,p4,p5,p6],'sum','upper link','lower link','tierod','caliper
upper','caliper lower','caliper dual')
axis([0,length(upp_link_force),-Inf,Inf])



figure
hold on
title('Moment magnitudes')
xlabel('loadstep')
ylabel('moment (Nmm)')
plot(sum_torque_mag,'w')
plot([limit(1),limit(1)],ylim,'Color',gray)
plot([limit(2),limit(2)],ylim,'Color',gray)
plot([limit(3),limit(3)],ylim,'Color',gray)
plot([limit(4),limit(4)],ylim,'Color',gray)
plot([limit(5),limit(5)],ylim,'Color',gray)
p1 = plot(upp_link_torque(:,1),'b');
p2 = plot(low_link_torque(:,1),'r');
p3 = plot(cal_rot_torque(:,1),'g');
p0 = plot(sum_torque_mag,'k');
legend([p0,p1,p2,p3],'sum','upper link','lower link','caliper dual')
axis([0,length(upp_link_force),-Inf,Inf])

jump=100;


sum_force_mag2 = sum_force_mag(1:jump:end,:);
sum_torque_mag2 = sum_torque_mag(1:jump:end,:);



figure
hold on
title('upper link force')
xlabel('loadstep')
ylabel('force (N)')
plot(upp_link_force(:,2),'w')
plot(upp_link_force(:,3),'w')
plot(upp_link_force(:,4),'w')
plot([limit(1),limit(1)],ylim,'Color',gray)
plot([limit(2),limit(2)],ylim,'Color',gray)
plot([limit(3),limit(3)],ylim,'Color',gray)
plot([limit(4),limit(4)],ylim,'Color',gray)
plot([limit(5),limit(5)],ylim,'Color',gray)
p1 = plot(upp_link_force(:,2),'b');
p2 = plot(upp_link_force(:,3),'r');
p3 = plot(upp_link_force(:,4),'g');
legend([p1,p2,p3],'x','y','z')
axis([0,length(upp_link_force),-Inf,Inf])

figure
hold on
title('lower link force')
```

```
xlabel('loadstep')
ylabel('force (N)')
plot(low_link_force(:,2),'w')
plot(low_link_force(:,3),'w')
plot(low_link_force(:,4),'w')
plot([limit(1),limit(1)],ylim,'Color',gray)
plot([limit(2),limit(2)],ylim,'Color',gray)
plot([limit(3),limit(3)],ylim,'Color',gray)
plot([limit(4),limit(4)],ylim,'Color',gray)
plot([limit(5),limit(5)],ylim,'Color',gray)
p1 = plot(low_link_force(:,2),'b');
p2 = plot(low_link_force(:,3),'r');
p3 = plot(low_link_force(:,4),'g');
legend([p1,p2,p3],'x','y','z')
axis([0,length(upp_link_force),-Inf,Inf])

figure
hold on
title('tierod force')
xlabel('loadstep')
ylabel('force (N)')
plot(tie_force(:,2),'w')
plot(tie_force(:,3),'w')
plot(tie_force(:,4),'w')
plot([limit(1),limit(1)],ylim,'Color',gray)
plot([limit(2),limit(2)],ylim,'Color',gray)
plot([limit(3),limit(3)],ylim,'Color',gray)
plot([limit(4),limit(4)],ylim,'Color',gray)
plot([limit(5),limit(5)],ylim,'Color',gray)
p1 = plot(tie_force(:,2),'b');
p2 = plot(tie_force(:,3),'r');
p3 = plot(tie_force(:,4),'g');
legend([p1,p2,p3],'x','y','z')
axis([0,length(upp_link_force),-Inf,Inf])

figure
hold on
title('caliper upper force')
xlabel('loadstep')
ylabel('force (N)')
plot(cal_upp_force(:,2),'w')
plot(cal_upp_force(:,3),'w')
plot(cal_upp_force(:,4),'w')
plot([limit(1),limit(1)],ylim,'Color',gray)
plot([limit(2),limit(2)],ylim,'Color',gray)
plot([limit(3),limit(3)],ylim,'Color',gray)
plot([limit(4),limit(4)],ylim,'Color',gray)
plot([limit(5),limit(5)],ylim,'Color',gray)
p1 = plot(cal_upp_force(:,2),'b');
p2 = plot(cal_upp_force(:,3),'r');
p3 = plot(cal_upp_force(:,4),'g');
legend([p1,p2,p3],'x','y','z')
axis([0,length(upp_link_force),-Inf,Inf])

figure
hold on
title('caliper lower force')
```

```
xlabel('loadstep')
ylabel('force (N)')
plot(cal_low_force(:,2),'w')
plot(cal_low_force(:,3),'w')
plot(cal_low_force(:,4),'w')
plot([limit(1),limit(1)],ylim,'Color',gray)
plot([limit(2),limit(2)],ylim,'Color',gray)
plot([limit(3),limit(3)],ylim,'Color',gray)
plot([limit(4),limit(4)],ylim,'Color',gray)
plot([limit(5),limit(5)],ylim,'Color',gray)
p1 = plot(cal_low_force(:,2),'b');
p2 = plot(cal_low_force(:,3),'r');
p3 = plot(cal_low_force(:,4),'g');
legend([p1,p2,p3],'x','y','z')
axis([0,length(upp_link_force),-Inf,Inf])

figure
hold on
title('caliper translational force')
xlabel('loadstep')
ylabel('force (N)')
plot(cal_trans_force(:,2),'w')
plot(cal_trans_force(:,3),'w')
plot(cal_trans_force(:,4),'w')
plot([limit(1),limit(1)],ylim,'Color',gray)
plot([limit(2),limit(2)],ylim,'Color',gray)
plot([limit(3),limit(3)],ylim,'Color',gray)
plot([limit(4),limit(4)],ylim,'Color',gray)
plot([limit(5),limit(5)],ylim,'Color',gray)
p1 = plot(cal_trans_force(:,2),'b');
p2 = plot(cal_trans_force(:,3),'r');
p3 = plot(cal_trans_force(:,4),'g');
legend([p1,p2,p3],'x','y','z')
axis([0,length(upp_link_force),-Inf,Inf])

figure
hold on
title('upper link torque')
xlabel('loadstep')
ylabel('force (Nmm)')
plot(upp_link_torque(:,2),'w')
plot(upp_link_torque(:,3),'w')
plot(upp_link_torque(:,4),'w')
plot([limit(1),limit(1)],ylim,'Color',gray)
plot([limit(2),limit(2)],ylim,'Color',gray)
plot([limit(3),limit(3)],ylim,'Color',gray)
plot([limit(4),limit(4)],ylim,'Color',gray)
plot([limit(5),limit(5)],ylim,'Color',gray)
p1 = plot(upp_link_torque(:,2),'b');
p2 = plot(upp_link_torque(:,3),'r');
p3 = plot(upp_link_torque(:,4),'g');
legend([p1,p2,p3],'x','y','z')
axis([0,length(upp_link_force),-Inf,Inf])

figure
hold on
title('lower link torque')
```

```
xlabel('loadstep')
ylabel('force (Nmm)')
plot(low_link_torque(:,2),'w')
plot(low_link_torque(:,3),'w')
plot(low_link_torque(:,4),'w')
plot([limit(1),limit(1)],ylim,'Color',gray)
plot([limit(2),limit(2)],ylim,'Color',gray)
plot([limit(3),limit(3)],ylim,'Color',gray)
plot([limit(4),limit(4)],ylim,'Color',gray)
plot([limit(5),limit(5)],ylim,'Color',gray)
p1 = plot(low_link_torque(:,2),'b');
p2 = plot(low_link_torque(:,3),'r');
p3 = plot(low_link_torque(:,4),'g');
legend([p1,p2,p3],'x','y','z')
axis([0,length(upp_link_force),-Inf,Inf])

figure
hold on
title('caliper rotational torque')
xlabel('loadstep')
ylabel('force (Nmm)')
plot(cal_rot_torque(:,2),'w')
plot(cal_rot_torque(:,3),'w')
plot(cal_rot_torque(:,4),'w')
plot([limit(1),limit(1)],ylim,'Color',gray)
plot([limit(2),limit(2)],ylim,'Color',gray)
plot([limit(3),limit(3)],ylim,'Color',gray)
plot([limit(4),limit(4)],ylim,'Color',gray)
plot([limit(5),limit(5)],ylim,'Color',gray)
p1 = plot(cal_rot_torque(:,2),'b');
p2 = plot(cal_rot_torque(:,3),'r');
p3 = plot(cal_rot_torque(:,4),'g');
legend([p1,p2,p3],'x','y','z')
axis([0,length(upp_link_force),-Inf,Inf])



% Validation code

format longE

upp_link_force = upp_link_force(:,2:4);
upp_link_torque = upp_link_torque(:,2:4);
low_link_force = low_link_force(:,2:4);
low_link_torque = low_link_torque(:,2:4);
tie_force = tie_force(:,2:4);
cal_upp_force = cal_upp_force(:,2:4);
cal_low_force = cal_low_force(:,2:4);
cal_trans_force = cal_trans_force(:,2:4);
cal_rot_torque = cal_rot_torque(:,2:4);



filename_val = 'loads_validation100.xlsx';
xlswrite(filename_val,upp_link_force,'upp_link_force')
xlswrite(filename_val,upp_link_torque,'upp_link_torque')
xlswrite(filename_val,low_link_force,'low_link_force')
```

```
xlswrite(filename_val,low_link_torque,'low_link_torque')
xlswrite(filename_val,tie_force,'tie_force')
xlswrite(filename_val,cal_upp_force,'cal_upp_force')
xlswrite(filename_val,cal_low_force,'cal_low_force')
xlswrite(filename_val,cal_trans_force,'cal_trans_force')
xlswrite(filename_val,cal_rot_torque,'cal_rot_torque')



% Code for chosing the worst load case

 [irrel,index] = max(sum_force_mag)

format longE

upp_link_force = upp_link_force(index,2:4);
upp_link_torque = upp_link_torque(index,2:4);
low_link_force = low_link_force(index,2:4);
low_link_torque = low_link_torque(index,2:4);
tie_force = tie_force(index,2:4);
cal_upp_force = cal_upp_force(index,2:4);
cal_low_force = cal_low_force(index,2:4);
cal_trans_force = cal_trans_force(index,2:4);
cal_rot_torque = cal_rot_torque(index,2:4);

data = {'upp_link_force',upp_link_force(1),upp_link_force(2),upp_link_force(3)
        'upp_link_torque',upp_link_torque(1),upp_link_torque(2),upp_link_torque(3)
        'low_link_force',low_link_force(1),low_link_force(2),low_link_force(3)
        'low_link_torque',low_link_torque(1),low_link_torque(2),low_link_torque(3)
        'tie_force',tie_force(1),tie_force(2),tie_force(3)
        'cal_upp_force',cal_upp_force(1),cal_upp_force(2),cal_upp_force(3)
        'cal_low_force',cal_low_force(1),cal_low_force(2),cal_low_force(3)
        'cal_trans_force',cal_trans_force(1),cal_trans_force(2),cal_trans_force(3)
        'cal_rot_torque',cal_rot_torque(1),cal_rot_torque(2),cal_rot_torque(3)};

filename = 'loads.xlsx';
xlswrite(filename,data)
```